bioRxiv preprint doi: https://doi.org/10.1101/2020.07.05.188557; this version posted July 5, 2020. The copyright holder for this preprint (which was not certified by peer review) is the author/funder, who has granted bioRxiv a license to display the preprint in perpetuity. It is made available under aCC-BY-NC-ND 4.0 International license.

Submitted *eLife*
2020-07-03

The ER membrane chaperone Shr3 co-translationally assists biogenesis of related plasma membrane transport proteins

Andreas Ring[§], Ioanna Myronidi[§] and Per O. Ljungdahl*

Department of Molecular Biosciences, The Wenner-Gren Institute, Stockholm University, SE-106 91, Sweden

Running title: Temporal aspects of membrane-localized chaperone assisted folding

Keywords: Shr3; membrane-localized chaperone; amino acid permease; polytopic membrane protein folding; endoplasmic reticulum; *Saccharomyces cerevisiae*

[§] Contributed equally.

[*] Corresponding author. Mailing address: Stockholm University, Department of Molecular Biosciences, The Wenner-Gren Institute, S-106 91 Stockholm, Sweden. Phone: 46 8 16 41 01. Fax: 46 8 16 42 09. E-mail: per.ljungdahl@su.se.

bioRxiv preprint doi: https://doi.org/10.1101/2020.07.05.188557; this version posted July 5, 2020. The copyright holder for this preprint (which was not certified by peer review) is the author/funder, who has granted bioRxiv a license to display the preprint in perpetuity. It is made available under aCC-BY-NC-ND 4.0 International license.

Abstract

Proteins with multiple membrane-spanning segments (MS) co-translationally insert into the endoplasmic reticulum (ER) membrane of eukaryotic cells. In *Saccharomyces cerevisiae*, Shr3 is an ER membrane-localized chaperone (MLC) that is specifically required for the functional expression of amino acid permeases (AAP), a family of eighteen transporters comprised of 12 MS. Here, comprehensive scanning mutagenesis and deletion analysis of Shr3, combined with a modified split-ubiquitin approach, were used to probe chaperone-substrate (Shr3-AAP) interactions *in vivo*. A surprisingly low level of sequence specificity in Shr3 underlies Shr3-AAP interactions, which initiate early as the first 2 MS of AAP partition into the membrane. The Shr3-AAP interactions successively strengthen and then weaken as all 12 MS partition into the membrane. Thus, Shr3 acts transiently in a co-translational manner to prevent MS of AAP translation intermediates from engaging in non-productive interactions, effectively preventing AAP misfolding during biogenesis.

Introduction

The integration and concomitant folding of membrane proteins in the lipid bilayer of the endoplasmic reticulum (ER) are critical steps in the biogenesis of transport proteins destined to function at the plasma membrane (PM). Most eukaryotic membrane proteins are co-translationally inserted into the ER membrane via the Sec61-complex, also known as the translocon. The translocon forms a protein-conducting aqueous channel that mediates protein translocation and the co-translational partitioning of membrane-spanning segments (MS) (Johnson and van Waes, 1999; Rapoport et al., 2017; Seinen and Driessen, 2019). During the synthesis of complex polytopic membrane proteins comprised of multiple MS, each MS exits from the aqueous channel and partitions into the ER membrane via the lateral gate of the translocon. Although the structural properties of the translocon indicate that the central channel is too small to accommodate multiple MS, the translocon appears to have a limited capacity to promote the folding of membrane proteins of lower complexity comprised of up to three MS; two separate extra-channel MS-binding sites have been reported to act in a chaperone-like manner to delay the release of N-terminal MS until translation is completed (Hou et al., 2012). However, as the complexity of membrane proteins grows beyond three MS, the challenge of preventing inappropriate interactions between incompletely translated nascent chains apparently exceeds the chaperone-like activity of the translocon. Specifically, during the translation of more complex polytopic membrane proteins, e.g., amino acid permeases, the N-

bioRxiv preprint doi: https://doi.org/10.1101/2020.07.05.188557; this version posted July 5, 2020. The copyright holder for this preprint (which was not certified by peer review) is the author/funder, who has granted bioRxiv a license to display the preprint in perpetuity. It is made available under aCC-BY-NC-ND 4.0 International license.

terminal MS partition into the membrane prior to the synthesis and partitioning of C-terminal MS. To prevent the MS of translation intermediates from entering non-productive folding pathways, discrete and highly specialized ER resident membrane proteins have been described in fungi that prevent misfolding of specific families of polytopic membrane proteins (Kota and Ljungdahl, 2005; Lau et al., 2000; Ljungdahl et al., 1992; Luo et al., 2002; Martínez and Ljungdahl, 2000, 2004; Sherwood and Carlson, 1999; Shurtleff et al., 2018).

Shr3, the most comprehensively studied of these specialized ER components, was identified as an integral membrane protein required for the functional expression of the conserved family of amino acid permeases (AAP) (Ljungdahl et al., 1992). The AAP family in *Saccharomyces cerevisiae*, belonging to the Amino acid-Polyamine-Organocation (APC) super-family of transporters (Gilstring and Ljungdahl, 2000; Jack et al., 2000; Saier, 2000; Wong et al., 2012), is comprised of 18 genetically distinct but structurally similar proteins with 12 MS. Shr3 is composed of 210 amino acids organized into two functional domains; a membrane domain with four MS and a hydrophilic cytoplasmically oriented C-terminal domain. Initially, Shr3 was recognized as an essential factor facilitating the packaging of AAP into ER-derived secretory vesicles (Kuehn et al., 1996), and it was found to be important for the proper presentation of ER-exit motifs, located within the hydrophilic C-terminal tails of AAP, to the inner COPII coatomer subunit Sec24 (Kuehn et al., 1998; Malkus et al., 2002; Miller et al., 2002; Miller et al., 2003). Additional data regarding the packaging activity of Shr3 included genetic and physical interactions of Shr3 with components of the COPII-coated vesicles (Gilstring et al., 1999). Also, it was shown that Shr3 facilitated ER-vesicle formation in close proximity to fully integrated and folded AAP (Gilstring and Ljungdahl, 2000; Gilstring et al., 1999) and hence Shr3 was designated a packaging chaperone. The ability of Shr3 to interact with COPII components is primarily linked to its hydrophilic C-terminal tail. Consistently, Shr3 was found to associate with newly synthesized Gap1 in transient manner, the interaction was reported to exhibit a half-life of approximately 15 min. The observed association with Gap1 was initially thought to occur post-translationally since Gap1 fully integrates into the ER-membrane with each MS correctly oriented independently of Shr3 (Gilstring and Ljungdahl, 2000). Also, the AAP that accumulate in the ER of *shr3*Δ strains do not activate the unfolded protein stress response (UPR) (Gilstring et al., 1999).

However, subsequent studies revealed that Shr3 has an important function that is separate from and precedes its packaging function. Consequently, the view of Shr3 evolved from being a packaging into a specialized membrane-localized chaperone that interacts early with substrate AAP during their co-translational insertion into the ER membrane (Kota et al., 2007; Kota and

bioRxiv preprint doi: https://doi.org/10.1101/2020.07.05.188557; this version posted July 5, 2020. The copyright holder for this preprint (which was not certified by peer review) is the author/funder, who has granted bioRxiv a license to display the preprint in perpetuity. It is made available under aCC-BY-NC-ND 4.0 International license.

Ljungdahl, 2005). In these studies, Shr3 was found to prevent the aggregation of AAP in the ER-membrane, a function associated with the N-terminal membrane domain of Shr3, comprised of four hydrophobic α-helices and three hydrophilic loops (Kota and Ljungdahl, 2005). Critical evidence demonstrating the importance of Shr3 in facilitating the folding of AAP includes the finding that co-expressed split N- and C-terminal portions of Gap1 assemble into a functional permease in a Shr3-dependent manner (Kota et al., 2007). The membrane domain of Shr3 is required and suffices to prevent aggregation of the first five MS of Gap1 enabling productive folding interactions with the C-terminal portions of Gap1. Similar to full-length Gap1, the N-terminal fragment displays an increased propensity to aggregate in membranes isolated from cells lacking Shr3, and importantly, its aggregation appeared not to be affected by the presence or absence of the C-terminal fragment. In marked contrast, the aggregation status of the C-terminal fragment was dependent on the presence of both Shr3 and the N-terminal fragment. Since the N- and C-terminal fragments individually insert into the membrane, Shr3 apparently can maintain the N-terminal fragment in a conformation that enables the C-terminal fragment to interact and assemble with it. Although direct physical interactions between Shr3 and substrate AAP have not been demonstrated, all available data is consistent with Shr3 interacting early with N-terminal MS as they co-translationally partition into the ER membrane.

During translocation, exclusively hydrophobic MS rapidly partition readily into the lipid phase of the membrane , whereas less hydrophobic MS containing (Heinrich et al., 2000) charged or polar residues partition into the membrane less readily and are retained in proximity to the translocon or to translocon associated proteins, e.g., TRAM (Heinrich and Rapoport, 2003). In analogy to TRAM, we posited that Shr3 facilitates the partitioning of MS of AAP containing charged or polar amino acid residues as they emerge from the translocon. According to this hypothesis, Shr3 may physically shield charged or polar residues within MS, thereby preventing these thermodynamically challenging segments from engaging in nonproductive interactions (Kota et al., 2007). More recent findings in yeast regarding the conserved ER membrane protein complex (EMC) have been interpreted in a similar manner (Shurtleff et al., 2018). However, a striking difference between Shr3 and EMC function is that null alleles of *SHR3* do not activate the UPR (Gilstring et al., 1999). Also, Shr3 has not been found to associate with EMC components, which contrasts to Gsf2, a MLC required for hexose transporter biogenesis (Kota and Ljungdahl, 2005; Sherwood and Carlson, 1999) and that apparently functions in association with the EMC (Shurtleff et al., 2018).

bioRxiv preprint doi: https://doi.org/10.1101/2020.07.05.188557; this version posted July 5, 2020. The copyright holder for this preprint (which was not certified by peer review) is the author/funder, who has granted bioRxiv a license to display the preprint in perpetuity. It is made available under aCC-BY-NC-ND 4.0 International license.

In summary, the available data regarding Shr3 are consistent with it having a dual role in the biogenesis of AAP, initially facilitating MS partitioning and folding, and subsequently, presenting native folded AAP as cargo during COPII vesicle formation. Despite the clear requirement of Shr3 in AAP biogenesis, we currently lack critical information regarding the mechanisms underlying Shr3 function. Here we have focused on the membrane domain of Shr3 and employed a comprehensive scanning mutagenesis approach to define amino acid residues involved in recognizing AAP substrates. Further, we have developed a split-ubiquitin approach to probe and characterize the temporal interactions with seven different AAP substrates *in vivo*. The data are consistent with Shr3 acting as a MLC providing a scaffold-like structure to help nascent chains of partially translated AAP maintain a structure required to enter and follow a productive folding pathway as translation proceeds to completion. Thus, Shr3 functions in a transient manner to facilitate the folding of AAP into native and functionally competent structures that can efficiently exit the ER.

Results

Systematic scanning mutagenesis of MS within the membrane domain of Shr3

We have previously shown that the membrane domain of Shr3 is required and sufficient for facilitating the folding of AAPs (Kota and Ljungdahl, 2005). To understand how Shr3 interacts with its AAP substrates, we employed a systematic scanning mutagenesis approach to identify residues within the Shr3 membrane domain required for function. Intramembrane residues were mutated to leucine; the length of consecutive substitution mutations varied, ranging from 2 to 13 residues. The extramembrane residues within ER lumenal loops L1 and L3 and cytoplasmic oriented NT and loop L2 where mutated to alanine; the length of consecutive alanine replacements ranged from 2 to 3.

The biological activity of the mutant proteins was initially assessed using growth-based assays on YPD supplemented with metsulfuron-methyl (MM), which provides a sensitive measure of Shr3 function. MM targets and inhibits branched-chain amino acid synthesis and growth is strictly dependent on the functional expression of amino acid permeases capable of facilitating high-affinity isoleucine, leucine and valine uptake (Jørgensen et al., 1998). Serial dilutions of cell suspensions from strain JKY2 (*shr3Δ*) carrying vector control (VC), *SHR3* or the *shr3* mutant alleles were spotted on YPD and YPD+MM plates (Supplementary Material Fig. S1 – S10). Only three mutant alleles, *shr3-35*, *shr3-50* and *shr3-76*, failed to support growth (Fig. 1A and B). The steady state levels of the three mutant proteins were similar to

bioRxiv preprint doi: https://doi.org/10.1101/2020.07.05.188557; this version posted July 5, 2020. The copyright holder for this preprint (which was not certified by peer review) is the author/funder, who has granted bioRxiv a license to display the preprint in perpetuity. It is made available under aCC-BY-NC-ND 4.0 International license.

wildtype Shr3 (Fig. 1B), suggesting that the mutant proteins were not grossly misfolded, and consequently, not prematurely targeted for ER-associated degradation.

The *shr3-35* allele encodes a protein with residues 17 through 19 (serine-alanine-threonine) in MS I replaced by leucine (Fig. 1A). To more precisely define the critical residues, we constructed additional mutant alleles with paired leucine substitutions at residues 17-18 (LLT), 18-19 (SLL) and 17 and 19 (LAL). Expression of *SHR3-36* (LLT) and *SHR3-38* (LAL) alleles complemented *shr3*Δ and supported wildtype growth on YPD + MM (Fig. 1C, dilutions 4 and 6). By contrast, cells expressing *shr3-37* (SLL) did not complement, exhibiting a phenotype similar to the *shr3-35* (LLL) mutant (Fig. 1C, dilutions 3 and 5).

The *shr3-76* allele carries leucine replacements at residues 139 through 142 (serine-asparagine-isoleucine-isoleucine) in MS IV (Fig. 1A). Again, the importance of the affected residues was tested by creating alleles with paired leucine substitutions at positions 139-140 (LLII) and 141-142 (SNLL). Cells expressing *shr3-77* (LLII) allele grew poorly, although slightly better than cells expressing the *shr3-76* allele (Fig. 1C, dilutions 15 and 16). Cells expressing *SHR3-78* (SNLL) grew as wildtype *SHR3* (Fig. 1C, dilutions 14 and 17).

The third non-functional allele, *shr3-50*, encodes a mutant protein with alanine substitutions at residues 51 through 53 (leucine-arginine-histidine) located within the ER lumenal loop L1 (Fig. 1A). The importance of these residues was tested by paired alanine substitutions of the positions 51-52 (AAH), 52-53 (LAA) and 51 and 53 (ARA). Expression of these alleles demonstrated that *SHR3-51* (AAH) and *SHR3-52* (LAA) complemented *shr3*Δ similar to wildtype *SHR3* (Fig.1C, dilutions 8, 10 and 11). The *shr3-53* (ARA) allele exhibited reduced growth (Fig. 1C, dilution 12), indicative of compromised function. The finding that mutations affecting residues 53-55 in the ER lumenal loop L1 abolish function suggests that extramembrane sequences are important for guiding the folding of AAP sequences destined to be oriented towards the extracellular side of the PM.

Deletion analysis of ER-lumen oriented loops

The possibility that Shr3 engages and interacts with its substrate AAP through contacts with extramembrane sequences prompted us to specifically test the functional significance of loops L1 and L3 (Fig. 2A). The residues 44-57 within L1 are predicted to fold into an amphipathic α-helix (Fig. 2B). We constructed four internal deletions in L1: *shr3*Δ*90* (Δ34-48); *shr3*Δ*91* (Δ39-47); *shr3*Δ*92* (Δ44-54); and *shr3*Δ*93* (Δ55-60); all of the L1 deletions affect this secondary structure motif to varying extent. Also, an internal deletion in L3 was constructed: *SHR3*Δ*94* (Δ121-127). The five deletion alleles directed the expression of mutant proteins at levels

bioRxiv preprint doi: https://doi.org/10.1101/2020.07.05.188557; this version posted July 5, 2020. The copyright holder for this preprint (which was not certified by peer review) is the author/funder, who has granted bioRxiv a license to display the preprint in perpetuity. It is made available under aCC-BY-NC-ND 4.0 International license.

comparable to *SHR3* (Fig. 2C); the deletions do not decrease the steady state levels of protein. The function of these deletion alleles was assessed as before using YPD + MM, which monitors the combined activity of multiple SPS-sensor regulated AAP (Andréasson and Ljungdahl, 2002; Jørgensen et al., 1998). We also extended the analysis with more nuanced growth-based assays capable of monitoring amino acid uptake catalyzed predominantly by a single or a couple of AAP. This was accomplished by examining growth on minimal media individually supplemented with toxic amino acid analogues D-histidine, L-canavanine, and azetidine-2-carboxylate (AzC), which are taken up by Gap1 (Gresham et al., 2010), Can1 (Ono et al., 1983), Agp1/Gnp1 (Andréasson et al., 2004), respectively. The expression of functional alleles of *SHR3* results in impaired growth in the presence of these toxic analogues. Serial dilutions of cell suspensions from strain JKY2 (*shr3Δ*) carrying vector control (VC), *SHR3*, *shr3Δ90*, *shr3Δ91*, *shr3Δ92*, *shr3Δ93* or *SHR3Δ94* were spotted on SAD containing D-histidine, SD + L-canavanine, SD + AzC, and YPD + MM plates. The four internal deletion alleles affecting L1 failed to complement *shr3Δ*; the strains grew similar as the VC (Fig. 2C, dilutions 1, 3, 4, 5 and 6). By contrast, the strain expressing the internal deletion in L3 showed more complex pattern of growth. On SAD + D-histidine and SD + L-canavanine, *SHR3Δ94* appeared to express a non-functional protein, the strain grew in the presence of these toxic amino acid analogues (Fig. 2C, compare dilution 1 with 7). However, on SD + AzC and YPD + MM, the *SHR3Δ94* allele exhibited growth similar to wildtype *SHR3* (Fig. 2C, compare dilution 2 with 7). Note that on YPD + MM the strain carrying *SHR3Δ94* exhibited enhanced growth compared to wildtype, and consequently, on YPD + MM we designated the phenotype WT^{+}.

Substrate specificity screen

The finding that *SHR3Δ94* exhibited a broad range of phenotypes, i.e., from null to apparently enhanced functionality, prompted us to reexamine the growth characteristics of the 44 leucine- and alanine-scanning mutant alleles using the nuanced growth-based assays. Serial dilutions of cell suspensions from strain JKY2 (*shr3Δ*) carrying vector control (VC), *SHR3* or one of the individual mutant alleles were spotted on SAD + D-histidine, SD + L-canavanine, SD + AzC and YPD+MM (Supplementary Material Fig. S1-S10). The growth characteristics were evaluated and the results, including the internal loop deletions, are summarized in an ordered heat-map (Fig. 3A). As was found in the initial evaluation of growth on YPD+MM, most of the mutant alleles were judged to encode functional proteins; the strains grew similarly as the strain carrying the *SHR3* wildtype control. Reevaluation of the three non-functional alleles, *shr3-35*, *shr3-50* and *shr3-76*, confirmed that the mutations exhibit major defects on all of the selective

bioRxiv preprint doi: https://doi.org/10.1101/2020.07.05.188557; this version posted July 5, 2020. The copyright holder for this preprint (which was not certified by peer review) is the author/funder, who has granted bioRxiv a license to display the preprint in perpetuity. It is made available under aCC-BY-NC-ND 4.0 International license.

media (Fig. 3A). However, in some instances, several of the mutations, similar to *SHR3Δ94*, conferred robust growth on YPD+MM but did not complement *shr3Δ* on the other selective media. Strikingly, *SHR3-45*, *-63*, *-65*, *-68*, *-71*, *-74*, and *-75*, supported more robust growth on YPD + MM than *SHR3*, but exhibited a null phenotype on media containing toxic amino acid analogues. In summary, growth in the presence of D-histidine was found to be the most sensitive monitor of mutations in *SHR3*, perhaps due to the fact that D-amino acids are taken up by a single AAP, Gap1 (Grenson et al., 1970; Rytka, 1975). We note that mutations localized to the MS III and IV and the ER lumenal oriented loop L3 exhibited the most pleiotropic affects, suggesting that these regions of Shr3 facilitate interactions with discrete AAP, and potentially, comprise substrate specific determinants.

We performed multiple sequence alignments of the membrane domain of Shr3 and orthologs from two *Saccharomyces sensu stricto* strains, *S. paradoxus* and *S. mikatae*, and from three divergent *lato* fungal strains, *Candida albicans* (Csh3), *Schizosaccharomyces pombe* (Psh3) and *Aspergillus nidulans* (ShrA) and obtained a consensus identity plot (Fig. 3B) (Madeira et al., 2019). The Shr3 orthologs of *C. albicans, S. pombe* and *A. nidulans* have been shown to function analogously and are required for proper amino acid uptake. Heterologous expression of *CHS3* complements *shr3Δ* (Martínez and Ljungdahl, 2004), whereas heterologous expression of *PHS3* or *SHRA* only partially complement *shr3Δ*, merely facilitating the functional expression of limited subset of permeases (Erpapazoglou et al., 2006; Martínez and Ljungdahl, 2000). The Shr3 sequence is well-conserved in the *Saccharomyces sensu stricto* strains, exhibiting almost absolute identity. Several positions throughout the membrane domain of Shr3 are conserved between the full set of selected sequences. Interestingly, threonine 19 which is the single critical amino acid residue in MS I is conserved in all selected sequences (Fig. 3B, T19 is highlighted in dark blue). The requirement for a polar amino acid in MS IV of Shr3 is conserved as well (Fig. 3B, S139 highlighted in dark blue). A higher sequence divergence is evident in the luminal loop L3, with the extreme case of the *A. nidulans* orthologue that contains an extra sequence of twelve amino acid residues. The limited sequence identity in loop L3 appears to be consistent with the observation that mutations in L3 of Shr3 exhibit the most pleiotropic effects, suggesting the existence of potential substrate specific determinants in this region.

The finding that the Shr3Δ94 mutation supported robust growth on YPD+MM, suggested that the mutant protein retained the capacity to facilitate Ssy1 folding. In contrast to the other members of the AAP transporter family, Ssy1 functions as the primary receptor of extracellular amino acids in the context of the plasma membrane-localized SPS sensor (Didion et al., 1998;

bioRxiv preprint doi: https://doi.org/10.1101/2020.07.05.188557; this version posted July 5, 2020. The copyright holder for this preprint (which was not certified by peer review) is the author/funder, who has granted bioRxiv a license to display the preprint in perpetuity. It is made available under aCC-BY-NC-ND 4.0 International license.

Iraqui et al., 1999; Klasson et al., 1999). In response to extracellular amino acids, Ssy1 initiates signaling events leading to the proteolytic activation of Stp1, which in turn induces the expression of several AAP genes including *AGP1* and *GNP1* and multiple permeases facilitating branched amino acid uptake. As an indirect measure of Shr3-Ssy1 interactions, we examined the proteolytic cleavage of the transcription factor Stp1 (Fig. 3C). Consistent with the growth assays, leucine induction led to Stp1 processing in strain FGY135 (*shr3Δ*) expressing *SHR3* or *SHR3Δ94* (Fig. 3C, lanes 4 and 8), but not the non-functional alleles *shr3-35*, *shr3-50* or *shr3-76* (Fig. 3C, lanes 6, 10 and 12).

Shr3-AAP substrate interactions

To test if the observed growth phenotypes of the mutated *SHR3*/*shr3* alleles correlated with the ability of mutant Shr3/shr3 proteins to interact with specific AAP and facilitate their functional expression we exploited a split-ubiquitin approach to monitor Shr3-AAP interactions *in vivo* (Fig. 4A and 4B). A sequence encoding the N-terminal fragment of ubiquitin carrying the I13A mutation (NubA), which reduces the propensity of non-specific interactions (Johnsson, 2002; Johnsson and Varshavsky, 1994), was fused at the C-terminal end of *SHR3*, *shr3-35*, and *SHR3Δ94*, creating the Shr3-NubA constructs schematically depicted in Fig. 4A. Next, we created a *GAP1* allele encoding the C-terminal fragment of ubiquitin (Cub) tagged with GST-6xHA (Cub-GST) (Fig. 4A). The resulting *GAP1-Cub-GST* was placed under the control of the *GAL1*-promoter. When co-expressed, productive interactions between Gap1 and Shr3 enable the split NubA and Cub domains to assemble a functional ubiquitin moiety that is recognized by ubiquitin-specific proteases, resulting in the release of the GST-6xHA reporter (Fig. 4B). The functional attributes of the NubA fusion constructs were tested by their ability to complement *shr3*Δ (Fig. 4C, dilutions 3-5); strains carrying *SHR3-NubA* or *SHR3Δ94-NubA* grew as well as *SHR3* without NubA (Fig. 4C, compare dilution 2 with 3 and 5), whereas the *shr3-35-NubA* allele did not (dilution 4). The *GAP1-Cub-GST* allele encodes a functional Gap1 protein that facilitates citrulline uptake as well as wildtype Gap1 (Fig. 4C, compare dilution 7 with 8). The functionality of Gap1-Cub-GST is dependent on its ability to exit the ER; a construct lacking the ER exit motif in the hydrophilic C-terminal domain of Gap1 is not functional (Fig. 4C dilution 9), presumably due its retention in the ER.

To test *in vivo* interactions, we grew strain FGY135 (*shr3Δ gap1Δ*) carrying plasmids *GAP1-Cub-GST* and *SHR3-NubA*, *shr3-35-NubA* or *SHR3-94-NubA* in synthetic media with 2% raffinose and 0.1% glucose. Cells from early logarithmic phase were collected and resuspended in synthetic media with 2% galactose for 1 hour at 30 °C. Protein extracts were prepared by

bioRxiv preprint doi: https://doi.org/10.1101/2020.07.05.188557; this version posted July 5, 2020. The copyright holder for this preprint (which was not certified by peer review) is the author/funder, who has granted bioRxiv a license to display the preprint in perpetuity. It is made available under aCC-BY-NC-ND 4.0 International license.

bead beating and analyzed using immunoblot analysis developed with anti-HA. In cells expressing *SHR3-NubA* or *SHR3-94-NubA* and *GAP1-Cub-GST-6xHA*, two bands were detected, corresponding to full-length Gap1-Cub-GST-6xHA and the cleaved GST-6xHA (Fig. 4D, lane 1). We calculated the fraction of split-ubiquitin cleavage in the *SHR3-NubA* strain to be ≈ 20% by dividing the intensities of the cleaved band with the intensities from full-length plus cleaved species; whereas in the *SHR3-94-NubA* strain the cleavage was 5% (Fig. 4D); By contrast, only a single band, full-length Gap1-Cub-GST-6xHA, was detected in extracts from the strain expressing the non-functional *shr3-35-NubA* and *GAP1-Cub-GST-6xHA* constructs (Fig. 4D, lane 2). Although expressed at similar levels, the ER retained gap1-ERX$_{AAA}$-Cub-Gst protein did not exhibit an enhanced propensity to interact with Shr3, indicating that the split-ubiquitin assay is specific (Fig. S11).

Based on the success of the split ubiquitin approach to analyze Shr3-Gap1 interactions, we created Cub-GST-6xHA tagged constructs with five additional AAP, i.e., Can1, Lyp1, Agp1, Gnp1 and Bap2 (Fig. 5A). Again, the goal was to test if the observed Shr3 wildtype and Shr3/shr3 mutant-dependent growth phenotypes correlated with specific Shr3-AAP interactions. Extracts from strain FGY135 (*shr3Δ gap1Δ*) carrying *SHR3-NubA*, *shr3-35-NubA* or *SHR3Δ94-NubA* and a single *AAP-Cub-GST-6xHA* construct were prepared and the levels of the GST-6xHA reporter were determined (Fig. 5B-D). Consistent with Shr3 being required for the efficient folding of AAP, we could detect robust interactions between each of the AAP-Cub constructs and wildtype Shr3-NubA. In contrast, AAP interactions with the non-functional shr3-35-NubA mutant were weak or absent, confirming that the approach was monitoring relevant interactions. Interestingly, the Shr3Δ94-NubA interacted with all AAP-Cub constructs, but at significantly reduced levels, and consequently, the data did not explain the enhanced growth conferred by the *SHR3Δ94-NubA* allele on YPD + MM (Fig. 2 and 3).

In an attempt to solve this conundrum, we considered the possibility that Shr3-Ssy1 interactions may provide the mechanistic basis of the observed phenotypes. Ssy1 is the integral membrane component of the PM-localized SPS sensor, which induces the expression of AAP genes in response to the presence of extracellular amino acids (Ljungdahl and Daignan-Fornier, 2012). Also, since Ssy1 is a unique member of the AAP family that strictly requires Shr3 for folding (Klasson et al., 1999), we reasoned that if the Shr3Δ94 mutant maintained the ability to assist the folding of Ssy1, then the transcriptional circuits, abrogated by *shr3*Δ would be restored and thereby increase the expression of multiple genes encoding AAP that facilitate branched-chain amino acids. Consistent with this notion, Shr3Δ94-NubA interacted with Ssy1-Cub-GST-6xHA at levels comparable to Shr3-NubA (Fig. 5E). Together our results correlate

bioRxiv preprint doi: https://doi.org/10.1101/2020.07.05.188557; this version posted July 5, 2020. The copyright holder for this preprint (which was not certified by peer review) is the author/funder, who has granted bioRxiv a license to display the preprint in perpetuity. It is made available under aCC-BY-NC-ND 4.0 International license.

well with the growth-based phenotypes, indicating that the interactions monitored by the split ubiquitin cleavage provide a nuanced assessment of Shr3-AAP interactions *in vivo*.

Temporal chaperone-substrate interactions

To investigate the temporal aspects of Shr3-facilitated AAP folding, we constructed a series of truncated *gap1-Cub-GST* alleles capable of encoding 2, 4, 6, 8, 10 and 12 MS (Fig. 6A). Strain FGY135 (*shr3Δ gap1Δ*) carrying plasmids *SHR3-NubA*, *shr3-35-NubA* or *SHR3Δ94-NubA* and a truncated *gap1-Cub-GST* allele was induced as described previously and potential interactions were monitored by immunoblot. Shr3-NubA and Shr3Δ94-NubA did not interact with gap1-2TM, even though the Cub domain is presented in the context of proper membrane topology oriented towards the cytoplasm (S12). The addition of two additional MS of Gap1 (gap1-4TM) supported an interaction with Shr3 (Fig. 6B, left and right panels). The intensity of the interactions increased and eventually plateaued in the strains carrying the gap1-6TM/-8TM/-10TM alleles, respectively (Fig. 6B, left and right panels). Although the interaction profiles are quite similar, in comparison to Shr3-Cub-GST, the interactions between Shr3Δ94-NubA and the gap1-Cub-GST constructs resulted in lower levels of the GST-6xHA reporter. Strikingly, the gap1-12TM construct interacted only weakly with the functional *SHR3* alleles (Fig. 6B, left and right panels). As expected, we failed to detect the GST-6xHA reporter in extracts from the strain expressing *shr3-35-NubA* (Fig. 6B, center panel).

In an analogous manner, we created a series of truncated Agp1 and Ssy1 split-ubiquitin constructs (Fig. 7A) and monitored potential interactions with Shr3-NubA, shr3-35-NubA or Shr3Δ94-NubA in strain FGY135 (*shr3Δ gap1Δ*). Interestingly, in contrast to gap1-2TM, the agp1-2TM construct clearly interacted with Shr3-NubA (Fig. 7A). Aside from this difference, the pattern of interactions with the remaining Agp1 constructs exhibited a striking similarity to that observed with Gap1 truncations; the intensity of the GST-6xHA interaction marker successively increased with increasing number of MS from 4 to 10, and was greatly reduced with the agp1-12TM construct (Fig. 7A). Notedly, the interaction pattern with the Ssy1 constructs was quite different (Fig. 7B). Interestingly, as did agp1-2TM, the ssy1-2TM interacted with Shr3-NubA, indicating that Shr3 engages early in the biogenesis of Ssy1. The ssy1-4TM and -6TM constructs exhibited weaker interactions, however, the ssy1-8TM, -10TM and -12TM constructs exhibited robust interactions. As anticipated from growth-based assays, Shr3Δ94-NubA exhibited an interaction pattern very similar to the wildtype Shr3-NubA construct, and interactions with the non-functional shr3-35-NubA construct were consistently weak.

bioRxiv preprint doi: https://doi.org/10.1101/2020.07.05.188557; this version posted July 5, 2020. The copyright holder for this preprint (which was not certified by peer review) is the author/funder, who has granted bioRxiv a license to display the preprint in perpetuity. It is made available under aCC-BY-NC-ND 4.0 International license.

Discussion

The initial stages of the biogenesis of AAP can be divided into three discrete functional steps, i.e., 1) integration into the ER membrane, 2) folding into native structures, and 3) packaging into ER-derived COPII-coated transport vesicles. Shr3 is not required for step 1, integration (Gilstring and Ljungdahl, 2000), but is required for folding and packaging into COPII-coated vesicles (Gilstring et al., 1999; Kuehn et al., 1998; Kuehn et al., 1996). Disruption of Shr3 function causes AAP to accumulate in the ER membrane with each MS properly integrated and oriented (Gilstring and Ljungdahl, 2000), but misfolded, resulting in high molecular weight aggregates that are subject to degradation by ER-associated degradation (ERAD) (Kota et al., 2007; Kota and Ljungdahl, 2005). Consequently, *shr3* null mutant strains exhibit a greatly diminished capacity to take up amino acids.

Here, our studies have been aimed at identifying the determinants in the membrane domain of Shr3 that underlie its role in facilitating AAP folding, i.e., its membrane-localized chaperone (MLC) function. To directly probe the *in vivo* interactions between Shr3 and AAP, and to characterize the temporal aspects of these interactions in the context of the native ER-membrane in living cells, we adapted and applied a split-ubiquitin approach that does not depend on a transcriptional readout. This approach proved to be a versatile tool enabling us to directly assess chaperone-substrate interactions. Our findings support the notion that Shr3 interacts very early during insertion of the first 2 to 4 MS of AAP into the ER membrane, presumably as they step-wise partition away from the Sec61 lateral gate. Hence, Shr3 appears to directly associate with nascent chains of AAP and does so in a transient manner consistent with the model depicted in Fig. 8. Our results implicate Shr3 as being situated in close proximity to the lateral gate of the translocon.

We performed saturation scanning mutagenesis of the N-terminal membrane domain of Shr3 to define the amino acid residues that participate in the recognition of AAP as folding substrates. Alanine and leucine residues were introduced in such a manner as to replace triplet residues, or longer strings of residues, of all of the native amino acids in hydrophilic loops and hydrophobic MS, respectively. The complete set of mutant proteins were tested for function using growth-based assays on media that allowed us to monitor the amino acid uptake activity of individual AAP, or a restricted set of multiple AAP, including those controlled by the SPS-sensor (Supplementary Material Fig. S1-S10; Fig. 3A). Strikingly, we found very limited sequence specific requirements for the Shr3 chaperone function. Mutations at only three sites

bioRxiv preprint doi: https://doi.org/10.1101/2020.07.05.188557; this version posted July 5, 2020. The copyright holder for this preprint (which was not certified by peer review) is the author/funder, who has granted bioRxiv a license to display the preprint in perpetuity. It is made available under aCC-BY-NC-ND 4.0 International license.

in MSI, L1 and MSIV resulted in a complete loss of function phenotype on all media tested, suggesting that Shr3 generally recognizes its folding substrates independently of sequence-specific interactions, but rather based on the presence of structural determinants shared by the AAP. Strikingly, two mutant proteins carrying 10 consecutive leucine residues (aa 62-71, Shr3-57, MSII) or 9 (aa 145-153, Shr3-79, MSIV) support functional expression of AAP in manner indistinguishable from wildtype Shr3, and the Shr3-58 mutant with 13 consecutive leucine residues (aa 69-81, MSII) functions well for all AAP except Gap1 (Fig. 3A, Fig. S6). These findings suggest that hydrophobic interactions between MS of Shr3 and AAP can develop even at the expense of larger sections of specific Shr3 sequence, presumably provided that its overall membrane structure is retained.

Very few critical residues were found in membrane segments. Interestingly, the critical residues identified in MSI and MSIV shared the common feature of being polar (Fig. 1C). Threonine19 is conserved among closely and more distant fungal species (Fig. 3B), and it is of interest to note that one of the original spontaneous mutations that led to the identification of *SHR3* is a T19R mutation (Ljungdahl et al., 1992). Together, the data suggest that Shr3 acts as a scaffold for AAP folding, a function that primarily depends on hydrophobic interactions but with the capacity to shield energetically unfavorable polar residues of AAP MS. This notion is supported by in vivo results demonstrating direct Shr3-AAP interactions with wildtype but not the non-functional MS I mutant shr3-35 (Fig. 4, Fig. 5). Importantly, exposed polar residues may be recognized by a hydrophilic pocket identified in the structure of the ERAD-associated E3 ubiquitin ligase Hrd1 (Schoebel et al., 2017), which is known to participate in the degradation of misfolded AAP in cells lacking Shr3 (Kota et al., 2007).

The finding that one of the three loss of function mutations globally disrupting Shr3 function resides in the lumen-oriented loop 1 (Fig. 1) suggests that Shr3 function is not solely dependent on MS-mediated hydrophobic interactions. Apparently, Shr3 facilitates the folding of AAP in a manner dependent on interactions between extramembrane lumen-oriented sequences. Consistent with this, all internal deletions in L1 of Shr3 strongly affected its function (Fig. 2). Interestingly, L1 contains a predicted α-helical structure with amphipathic characteristics (aa 44-57) that is disrupted in each of the internal deletion mutant proteins.

In contrast to the deletions in L1, a deletion affecting L3 exhibited pleiotropic effects (Fig. 2) that we traced to differential interactions with distinct AAP substrates, suggesting that L3 is an important determinant affecting substrate interactions. Indeed, this region appears to be critical for interactions with Gap1 and Can1, but less important for interactions with Agp1/Gnp1, and clearly dispensable for interactions with Ssy1 (Fig. 2, Fig. 4, Fig. 5).

bioRxiv preprint doi: https://doi.org/10.1101/2020.07.05.188557; this version posted July 5, 2020. The copyright holder for this preprint (which was not certified by peer review) is the author/funder, who has granted bioRxiv a license to display the preprint in perpetuity. It is made available under aCC-BY-NC-ND 4.0 International license.

Consistently, some mutations in *SHR3* result in WT+ phenotypes, i.e., exhibiting more robust growth than wildtype (Fig. 3A). This latter gain-of-function phenotype is presumably due to that Ssy1 folds properly, and thus, cells remain capable of inducing AAP gene expression in a manner that is augmented by the derepression of nitrogen regulation (Ljungdahl and Daignan-Fornier, 2012). Thus, under the specific growth conditions used, cells carrying L3 mutations express enhanced levels of AAP leading to WT+ growth.

The finding that Ssy1, the only non-transporting AAP, uniquely exhibits a lax requirement for L3 to fold, suggests that transporting AAP may have an enhanced requirement for the chaperone function of Shr3. This notion is consistent with recent evidence showing that the extracellular loops of AAP do not merely serve as MS-connecting sequences but hold important roles in the intracellular trafficking as well as transport function (van't Klooster et al., 2020). Some of the loops are of considerable length, especially extracellular loops 3 and 4 connecting MS V-VI and VII-VIII, respectively. Secondary structure predictions suggest the extracellular loops 4 of the lysine permease Lyp1 (van't Klooster et al., 2020) and Gap1 (Ghaddar et al., 2014a) possess α-helical regions that appear to influence the substrate specificity for amino acid transport (Risinger et al., 2006). The loop regions that are destined to face the extracellular milieu are ER lumen-oriented during AAP biogenesis, which is consistent with a requirement for chaperone-assisted folding dependent on the lumen-oriented loops of Shr3. Alternatively, the interactions with the lumen-oriented loops of Shr3 are required to maintain the extracellular regions of AAP flexible in a manner that allows proper interactions between MS as they partition out of the translocon gate into the ER membrane.

Although no Shr3 homologues have been identified in metazoans, the closest AAP homologues in mammals are L-type amino acid transporters (LAT) (SLC7 family). SLC7 transporters heterodimerize with 4F2hc or rBAT, members of the SLC3 protein family. SLC7-SLC3 heterodimerization is required for proper trafficking and functional expression of the holo-LAT transporters at the plasma membrane (Fotiadis et al., 2013). Crucially, the interaction is mediated through the extracellular regions of the two monomers and hints that a common hydrophobic patch in the extracellular portion of the SLC7 subunits serves as a substrate determinant for the recognition by the SLC3 subunit (Rosell et al., 2014). Although this hydrophobic patch is not well-conserved in cyanobacterial, yeast or fungal SLC7 homologues, the principle underlying the SLC7-SLC3 interaction is in line with the concept of extramembrane regions containing motifs for substrate recognition and specificity.

Although there is no crystal structure of an AAP, Bap2 (Usami et al., 2014), Can1 (Ghaddar et al., 2014a), Gap1 (Ghaddar et al., 2014b) and Tat2 (Kanda and Abe, 2013) have been

bioRxiv preprint doi: https://doi.org/10.1101/2020.07.05.188557; this version posted July 5, 2020. The copyright holder for this preprint (which was not certified by peer review) is the author/funder, who has granted bioRxiv a license to display the preprint in perpetuity. It is made available under aCC-BY-NC-ND 4.0 International license.

successfully modeled onto the *E. coli* arginine/agmatine antiporter AdiC (Gao et al., 2010). AdiC has 12 MS and belongs to the Amino Acid-Polyamine-Organocation (APC) super-family of transporters. The 12 MS are arranged in a 5+5 inverted repeat fold that form the transporter core, with MS XI and XII appearing to hold the two halves together. MS I, III, VI, VIII and X shape the binding pocket. Accordingly, we find that the pattern of interactions between Shr3 and Gap1 and Agp1 intermediates is striking (Fig.6). Interactions are robust when the first half of the permease is translated. As more MS are added enabling the 5+5 fold, the interaction increases and plateaus until the presence of MS XII, when interaction is severely reduced. The difference in Ssy1 (Fig. 7) could perhaps be attributed to that it is a non-transporting AAP. Together, the data we acquired in this study provide further support to our previously described model (Kota et al., 2007; Kota and Ljungdahl, 2005) whereby Shr3 interacts with AAP early as they partition into the ER membrane to act as an assembly site for MS helices and provide a protective environment for AAP translation intermediates to avoid nonproductive interactions while shielding polar residues, until all MS are available to form the long-range intramolecular interactions that characterize the native AAP 3D-structure (Fig.8). A similar function as an assembly site for alpha helices of polytopic membrane proteins had been previously proposed for the bacterial insertase/chaperone YidC (Beck et al., 2001). Aside from its well-described function in membrane protein insertion and assembly (Dalbey and Kuhn, 2014), YidC is required for folding of the polytopic membrane proteins LacY and MalF (Nagamori et al., 2004; Serdiuk et al., 2016; Serdiuk et al., 2019; Wagner et al., 2008; Zhu et al., 2013). Our model for the Shr3 chaperone function in the biogenesis of AAP is analogous to that of YidC in the folding of LacY where hydrophobic interactions mediate shielding of LacY, providing a protective chamber that reduces energetically unfavorable contacts in the non-native structure during translation (Zhu et al., 2013)

More recently, the conserved eukaryotic ER membrane protein complex (EMC) has been implicated in various roles facilitating membrane protein biogenesis (Volkmar and Christianson, 2020), including those of a MS insertase (Chitwood et al., 2018; Guna et al., 2018) and a chaperone-like capacity for diverse polytopic membrane proteins (Shurtleff et al., 2018). Although mechanistic details of how the EMC exerts its chaperone-like function remain to be elucidated, it apparently acts in close proximity with nascent polytopic membrane proteins typically enriched for MS containing polar or charged residues (Shurtleff et al., 2018). Importantly, the EMC can associate with a number of ER-integral substrate-specific chaperones such as Sop4 (Luo et al., 2002), Gsf2 (Kota and Ljungdahl, 2005; Sherwood and Carlson, 1999) and Ilm1 (Shurtleff et al., 2018). The polytopic membrane proteins Pma1, Hxt1 and Fks1 are

bioRxiv preprint doi: https://doi.org/10.1101/2020.07.05.188557; this version posted July 5, 2020. The copyright holder for this preprint (which was not certified by peer review) is the author/funder, who has granted bioRxiv a license to display the preprint in perpetuity. It is made available under aCC-BY-NC-ND 4.0 International license.

respective substrates of these membrane-localized chaperones and show increased association with the EMC upon deletion of their specific membrane-localized chaperone. Interestingly, the AAP Hip1 has been classified among the putative EMC clients, however none of the remaining 17 members of the yeast AAP family have been implicated as clients. Importantly, Shr3, although an abundant ER membrane protein, has not been found to interact with EMC components (Shurtleff et al., 2018). Consistent with Shr3 acting independent of EMC, Gap1 is not affected by the loss of a more specialized, but stoichiometric, component of the EMC (Sop4/EMC7), which induces a newly described pre-emptive quality control mechanism leading to translational arrest specifically at ribosomes translating a misfolded EMC7 substrate (Lakshminarayan et al., 2020).

Finally, in previous experiments and here (Fig. 3A) we have shown that the functional expression of Gap1 at the plasma membrane is highly dependent on Shr3 (Gilstring et al., 1999; Kota et al., 2007; Kota and Ljungdahl, 2005; Ljungdahl et al., 1992). Gap1, but not the hexose transporter Hxt1, is packaged in ER-derived vesicles that contain the glycosylated α-factor precursor (gpaF), indicating that gpaF and Hxt1 are not concentrated at the same ER-exit sites (ERES) (Castillon et al., 2009). Based on these observations, it is also unlikely that Gap1 and Hxt1 are concentrated at the same ERES. In contrast to Shr3, the hexose transporter-specific MLC Gsf2 is thought to interact with the EMC, suggesting that the EMC and Shr3 facilitate membrane protein biogenesis in different microenvironments within the ER membrane. We find it attractive to postulate the existence of populations of ribosomes functioning in the proximity of different sets of biogenesis factors, which would facilitate the incorporation of discrete substrates into distinct ER-derived vesicles. This could function in synchrony with the Sec61 translocon pairing up with diverse sets of partners to efficiently insert or translocate more challenging versus canonical substrates of the secretory pathway in and across the ER-membrane (O'Keefe and High, 2020). In the case of Shr3, the early interactions with nascent AAP being inserted in the lipid bilayer together with the ability of Shr3 to interact with COPII components via its C-terminal cytoplasmic tail (Gilstring et al., 1999), converge to a function as a nexus between AAP folding and packaging into COPII-coated vesicles. The potential network of dynamic interactions in the ER remains to be explored for an integral substrate-specific chaperone as well as what structural determinants in the substrates dictate a remarkable degree of substrate specificity. To this end, the approaches described here in combination with high-resolution assays to probe protein-protein interactions can find application.

Materials and methods

bioRxiv preprint doi: https://doi.org/10.1101/2020.07.05.188557; this version posted July 5, 2020. The copyright holder for this preprint (which was not certified by peer review) is the author/funder, who has granted bioRxiv a license to display the preprint in perpetuity. It is made available under aCC-BY-NC-ND 4.0 International license.

Yeast strains and plasmids

Yeast strains and plasmid used are listed in Supplementary Material Tables S1 and S2, respectively.

Media

Standard media, YPD (yeast extract, peptone, dextrose), SD (synthetic defined with ammonium as nitrogen source and glucose as carbon source) were prepared as previously described (Burke et al., 2000). Ammonia-based synthetic complete dextrose (SC) drop-out medium, were prepared as described (Andréasson and Ljungdahl, 2002) and SAD (synthetic minimal dextrose, with allantoin as sole nitrogen source) was prepared as previously described. Media were made solid with 2% (wt/vol) bacto Agar (Difco), 2% (wt/vol) washed bacto Agar (Difco) or 2% (wt/vol) washed pure Agar where indicated. Sensitivity to 200 µg/ml MM (metsulfuron-methyl = 2-{[({[(4-methoxy-6-methyl)-1,3,5-triazin-2-yl]-amino}carbonyl) amino-]-sulfonyl}-benzoic acid) was tested on YPD as described previously (Jørgensen et al., 1998). Sensitivity to 1 mM AzC (azetidine-2-carboxylate), 10 µg/ml DL-ethionine, 50 µg/ml p-Fluoro-DL-phenylalanine and 1 µg/ml L-canavanine was tested on SD. Sensitivity to 0,5% (wt/vol) D-histidine was tested on SAD media made solid with washed pure Agar. Cells were grown over night in SC-uracil medium, cells were then resuspended in water to OD=1, 10-fold dilutions were prepared in water and then spotted on the indicated medium. Plates were then incubated at 30°C for 2–3 d and photographed. Gap1-dependent citrulline uptake was monitored on minimal medium containing 2 % galactose as carbon source, 1 mM L-citrulline as sole nitrogen source and uracil. Media were made solid with washed bacto Agar. Plates were incubated at 30 °C for 7 d and photographed.

Immunoblot analysis

Whole-cell extracts were prepared under denaturing conditions using NaOH and trichloroacetic acid as described previously (Silve et al., 1991). Proteins were separated using SDS-PAGE and blotted onto Amersham Protran 0.45 µm nitrocellulose membrane (GE Healthcare). The primary antibodies and dilutions were, mouse anti-Dpm1 5C5A7 (Abcam), 1:2500; rat anti-HA-HRP 3F10 (Roche Applied Science), 1:2500-1:5000; mouse anti-Pgk1 22C5D8 (Thermo Fisher Scientific), 1:10000 and rabbit anti-Shr3, 1:9000. Secondary antibodies and dilutions used were, goat anti-mouse-poly-HRP (Thermo Fisher Scientific), 1:5000 and goat anti-rabbit-poly-HRP (Thermo Fisher Scientific), 1:5000. Immunoreactive bands were visualized by

bioRxiv preprint doi: https://doi.org/10.1101/2020.07.05.188557; this version posted July 5, 2020. The copyright holder for this preprint (which was not certified by peer review) is the author/funder, who has granted bioRxiv a license to display the preprint in perpetuity. It is made available under aCC-BY-NC-ND 4.0 International license.

chemiluminescence using (SuperSignal West Dura Extended-Duration Substrate; Thermo Fisher Scientific) as substrate in a ChemiDoc imaging system (Biorad).

Split-ubiquitin assay

Cells were pre-grown in SD+R (synthetic defined with ammonium as nitrogen source and 2 % raffinose and 0.1 % glucose as carbon source) to logarithmic phase. Approximately 10 OD of logarithmically cells were induced in 5 ml of SD+G (synthetic defined with ammonium as nitrogen source and 2 % galactose as carbon source) for 1 hour. Cells were collected and washed once in ddH_20. Cells were resuspended in 150 µl lysis buffer (0.8 M sorbitol; 10 mM MOPS, pH 7.2; 2 mM EDTA; 1 mM PMSF; 1X cØmplete, mini, EDTA-free protease inhibitor cocktail, Roche). Cells were lysed by bead beating with 0.5 mm glass beads for 3x20s at 6.5 m/s in a benchtop homogenizer (Fastprep-24, MP Biomedical). The cell lysates were centrifuged at 500g for 10 min and 25 µl of the resulting supernatant was diluted 1:1 with 2x sample buffer. Proteins were separated using SDS-PAGE and blotted onto Amersham Protran 0.45 µm nitrocellulose membrane (GE Healthcare). The primary antibody and dilution used was rat anti-HA-HRP 3F10 (Roche Applied Science), 1:2500-1:5000. Immunoreactive bands were visualized by chemiluminescence using (SuperSignal West Dura Extended-Duration Substrate; Thermo Fisher Scientific) as substrate in a ChemiDoc imaging system (Biorad).

Protease protection assay

Cells were pre-grown in SD+R (synthetic defined with ammonium as nitrogen source and 2 % raffinose and 0.1 % glucose as carbon source) to logarithmic phase. Approximately 5 OD of logarithmically cells were induced in 5 ml of SD+G (synthetic defined with ammonium as nitrogen source and 2 % galactose as carbon source) for 1 hour. Cells were collected and washed once in ddH_20. Cells were resuspended in 150 µl lysis buffer (0.8 M sorbitol; 10 mM MOPS, pH 7.2; 2 mM EDTA; 1 mM PMSF; 1X cØmplete, mini, EDTA-free protease inhibitor cocktail, Roche). Cells were lysed by bead beating with 0.5 mm glass beads for 3x20s at 6.5 m/s in a benchtop homogenizer (Fastprep-24, MP Biomedical). The cell lysates were centrifuged at 500g for 10 min and 100 µl of the resulting supernatant was centrifuged at 100 000 g for 30 minutes. The membrane pellet was resuspended in 50 µl lysis buffer (0.8 M sorbitol; 10 mM MOPS, pH 7.2; 2 mM EDTA; 5 mM $CaCl_2$). The resulting membrane preparations were digested with addition of 20 µg Proteinase K (Thermo Fisher Scientific) and 0.2 % NP-40 where indicated on ice. Time points where taken at 0 and 2 h. Proteins were precipitated using trichloroacetic acid as described previously (Silve et al., 1991). Proteins were separated using

bioRxiv preprint doi: https://doi.org/10.1101/2020.07.05.188557; this version posted July 5, 2020. The copyright holder for this preprint (which was not certified by peer review) is the author/funder, who has granted bioRxiv a license to display the preprint in perpetuity. It is made available under aCC-BY-NC-ND 4.0 International license.

SDS-PAGE and blotted onto Amersham Protran 0.45 µm nitrocellulose membrane (GE Healthcare). The primary antibodies and dilutions used were, rat anti-HA-HRP 3F10 (Roche Applied Science), 1:2500-1:5000 and rabbit anti-Kar2, 1:5000. Secondary antibody and dilution used was goat anti-rabbit-poly-HRP (Thermo Fisher Scientific), 1:5000. Immunoreactive bands were visualized by chemiluminescence using (SuperSignal West Dura Extended-Duration Substrate; Thermo Fisher Scientific) as substrate in a ChemiDoc imaging system (Biorad).

Acknowledgements

We thank the members of the Ljungdahl laboratory and Claes Andréasson for constructive comments throughout the course of this work. In particular we acknowledge Nina Horwege, and Carlos Sacristán for early contributions in creating plasmid constructs. This research was supported by funding from Swedish Research Council (P.O.L.), Grant/Award numbers: 2011-5925 and 2015-04202.

Competing interests

The authors have no conflicts of interest to report.

References

Andréasson, C., and Ljungdahl, P.O. (2002). Receptor-mediated endoproteolytic activation of two transcription factors in yeast. Genes Dev *16*, 3158-3172.

Andréasson, C., Neve, E.P.A., and Ljungdahl, P.O. (2004). Four permeases import proline and the toxic proline analogue azetidine-2-carboxylate into yeast. Yeast *21*, 193-199.

Beck, K., Eisner, G., Trescher, D., Dalbey, R.E., Brunner, J., and Muller, M. (2001). YidC, an assembly site for polytopic Escherichia coli membrane proteins located in immediate proximity to the SecYE translocon and lipids. EMBO Rep *2*, 709-714.

Castillon, G.A., Watanabe, R., Taylor, M., Schwabe, T.M., and Riezman, H. (2009). Concentration of GPI-anchored proteins upon ER exit in yeast. Traffic *10*, 186-200.

Chitwood, P.J., Juszkiewicz, S., Guna, A., Shao, S., and Hegde, R.S. (2018). EMC Is Required to Initiate Accurate Membrane Protein Topogenesis. Cell *175*, 1507-1519 e1516.

Dalbey, R.E., and Kuhn, A. (2014). How YidC inserts and folds proteins across a membrane. Nat Struct Mol Biol *21*, 435-436.

Didion, T., Regenberg, B., Jørgensen, M.U., Kielland-Brandt, M.C., and Andersen, H.A. (1998). The permease homologue Ssy1p controls the expression of amino acid and peptide transporter genes in *Saccharomyces cerevisiae*. Mol Microbiol *27*, 643-650.

bioRxiv preprint doi: https://doi.org/10.1101/2020.07.05.188557; this version posted July 5, 2020. The copyright holder for this preprint (which was not certified by peer review) is the author/funder, who has granted bioRxiv a license to display the preprint in perpetuity. It is made available under aCC-BY-NC-ND 4.0 International license.

Drozdetskiy, A., Cole, C., Procter, J., and Barton, G.J. (2015). JPred4: a protein secondary structure prediction server. Nucleic Acids Res *43*, W389-394.

Erpapazoglou, Z., Kafasla, P., and Sophianopoulou, V. (2006). The product of the SHR3 orthologue of Aspergillus nidulans has restricted range of amino acid transporter targets. Fungal Genet Biol *43*, 222-233.

Forsberg, H., and Ljungdahl, P.O. (2001). Genetic and biochemical analysis of the yeast plasma membrane Ssy1p-Ptr3p-Ssy5p sensor of extracellular amino acids. Mol Cell Biol *21*, 814-826.

Fotiadis, D., Kanai, Y., and Palacin, M. (2013). The SLC3 and SLC7 families of amino acid transporters. Mol Aspects Med *34*, 139-158.

Gao, X., Zhou, L., Jiao, X., Lu, F., Yan, C., Zeng, X., Wang, J., and Shi, Y. (2010). Mechanism of substrate recognition and transport by an amino acid antiporter. Nature *463*, 828-832.

Ghaddar, K., Krammer, E.M., Mihajlovic, N., Brohee, S., Andre, B., and Prevost, M. (2014a). Converting the yeast arginine can1 permease to a lysine permease. J Biol Chem *289*, 7232-7246.

Ghaddar, K., Merhi, A., Saliba, E., Krammer, E.M., Prevost, M., and Andre, B. (2014b). Substrate-induced ubiquitylation and endocytosis of yeast amino acid permeases. Mol Cell Biol *34*, 4447-4463.

Gilstring, C.F., and Ljungdahl, P.O. (2000). A method for determining the in vivo topology of yeast polytopic membrane proteins demonstrates that Gap1p fully integrates into the membrane independently of Shr3p. J Biol Chem *275*, 31488-31495.

Gilstring, C.F., Melin-Larsson, M., and Ljungdahl, P.O. (1999). Shr3p mediates specific COPII coatomer-cargo interactions required for the packaging of amino acid permeases into ER-derived transport vesicles. Mol Biol Cell *10*, 3549-3565.

Grenson, M., Hou, C., and Crabeel, M. (1970). Multiplicity of the amino acid permeases in Saccharomyces cerevisiae. IV. Evidence for a general amino acid permease. J Bacteriol *103*, 770-777.

Gresham, D., Usaite, R., Germann, S.M., Lisby, M., Botstein, D., and Regenberg, B. (2010). Adaptation to diverse nitrogen-limited environments by deletion or extrachromosomal element formation of the GAP1 locus. Proc Natl Acad Sci U S A *107*, 18551-18556.

Guna, A., Volkmar, N., Christianson, J.C., and Hegde, R.S. (2018). The ER membrane protein complex is a transmembrane domain insertase. Science *359*, 470-473.

Heinrich, S.U., Mothes, W., Brunner, J., and Rapoport, T.A. (2000). The Sec61 complex mediates the integration of a membrane protein by allowing lipid partitioning of the transmembrane domain. Cell *102*, 233-244.

Heinrich, S.U., and Rapoport, T.A. (2003). Cooperation of transmembrane segments during the integration of a double-spanning protein into the ER membrane. Embo J *22*, 3654-3663.

Hou, B., Lin, P.J., and Johnson, A.E. (2012). Membrane protein TM segments are retained at the translocon during integration until the nascent chain cues FRET-detected release into bulk lipid. Mol Cell *48*, 398-408.

Iraqui, I., Vissers, S., Bernard, F., de Craene, J.O., Boles, E., Urrestarazu, A., and André, B. (1999). Amino acid signaling in *Saccharomyces cerevisiae*: a permease-like sensor of external amino acids and F-Box protein Grr1p are required for transcriptional induction of the *AGP1* gene, which encodes a broad-specificity amino acid permease. Mol Cell Biol *19*, 989-1001.

bioRxiv preprint doi: https://doi.org/10.1101/2020.07.05.188557; this version posted July 5, 2020. The copyright holder for this preprint (which was not certified by peer review) is the author/funder, who has granted bioRxiv a license to display the preprint in perpetuity. It is made available under aCC-BY-NC-ND 4.0 International license.

Jack, D.L., Paulsen, I.T., and Saier, M.H. (2000). The amino acid/polyamine/organocation (APC) superfamily of transporters specific for amino acids, polyamines and organocations. Microbiology *146 (Pt 8)*, 1797-1814.

Johnson, A.E., and van Waes, M.A. (1999). The translocon: a dynamic gateway at the ER membrane. Annu Rev Cell Dev Biol *15*, 799-842.

Johnsson, N. (2002). A split-ubiquitin-based assay detects the influence of mutations on the conformational stability of the p53 DNA binding domain in vivo. FEBS Lett *531*, 259-264.

Johnsson, N., and Varshavsky, A. (1994). Split ubiquitin as a sensor of protein interactions in vivo. Proc Natl Acad Sci U S A *91*, 10340-10344.

Jørgensen, M.U., Bruun, M.B., Didion, T., and Kielland-Brandt, M.C. (1998). Mutations in five loci affecting GAP1-independent uptake of neutral amino acids in yeast. Yeast *14*, 103-114.

Kanda, N., and Abe, F. (2013). Structural and functional implications of the yeast high-affinity tryptophan permease Tat2. Biochemistry *52*, 4296-4307.

Klasson, H., Fink, G.R., and Ljungdahl, P.O. (1999). Ssy1p and Ptr3p are plasma membrane components of a yeast system that senses extracellular amino acids. Mol Cell Biol *19*, 5405-5416.

Kota, J., Gilstring, C.F., and Ljungdahl, P.O. (2007). Membrane chaperone Shr3 assists in folding amino acid permeases preventing precocious ERAD. J Cell Biol *176*, 617-628.

Kota, J., and Ljungdahl, P.O. (2005). Specialized membrane-localized chaperones prevent aggregation of polytopic proteins in the ER. J Cell Biol *168*, 79-88.

Kuehn, M.J., Herrmann, J.M., and Schekman, R. (1998). COPII-cargo interactions direct protein sorting into ER-derived transport vesicles. Nature *391*, 187-190.

Kuehn, M.J., Schekman, R., and Ljungdahl, P.O. (1996). Amino acid permeases require COPII components and the ER resident membrane protein Shr3p for packaging into transport vesicles in vitro. J Cell Biol *135*, 585-595.

Lakshminarayan, R., Phillips, B.P., Binnian, I.L., Gomez-Navarro, N., Escudero-Urquijo, N., Warren, A.J., and Miller, E.A. (2020). Pre-emptive Quality Control of a Misfolded Membrane Protein by Ribosome-Driven Effects. Curr Biol *30*, 854-864 e855.

Lau, W.T., Howson, R.W., Malkus, P., Schekman, R., and O'Shea, E.K. (2000). Pho86p, an endoplasmic reticulum (ER) resident protein in *Saccharomyces cerevisiae*, is required for ER exit of the high-affinity phosphate transporter Pho84p. Proc Natl Acad Sci USA *97*, 1107-1112.

Ljungdahl, P.O., and Daignan-Fornier, B. (2012). Regulation of amino acid, nucleotide, and phosphate metabolism in Saccharomyces cerevisiae. Genetics *190*, 885-929.

Ljungdahl, P.O., Gimeno, C.J., Styles, C.A., and Fink, G.R. (1992). SHR3: A novel component of the secretory pathway specifically required for the localization of amino acid permeases in yeast. Cell *71*, 463-478.

Luo, W.J., Gong, X.H., and Chang, A. (2002). An ER membrane protein, Sop4, facilitates ER export of the yeast plasma membrane [H+]ATPase, Pma1. Traffic *3*, 730-739.

Madeira, F., Park, Y.M., Lee, J., Buso, N., Gur, T., Madhusoodanan, N., Basutkar, P., Tivey, A.R.N., Potter, S.C., Finn, R.D.*, et al.* (2019). The EMBL-EBI search and sequence analysis tools APIs in 2019. Nucleic Acids Research *47*, W636-W641.

bioRxiv preprint doi: https://doi.org/10.1101/2020.07.05.188557; this version posted July 5, 2020. The copyright holder for this preprint (which was not certified by peer review) is the author/funder, who has granted bioRxiv a license to display the preprint in perpetuity. It is made available under aCC-BY-NC-ND 4.0 International license.

Malkus, P., Jiang, F., and Schekman, R. (2002). Concentrative sorting of secretory cargo proteins into COPII-coated vesicles. J Cell Biol *159*, 915-921.

Martínez, P., and Ljungdahl, P.O. (2000). The SHR3 homologue from *S. pombe* demonstrates a conserved function of ER packaging chaperones. J Cell Sci *113*, 4351-4362.

Martínez, P., and Ljungdahl, P.O. (2004). An ER packaging chaperone determines the amino acid uptake capacity and virulence of *Candida albicans*. Mol Microbiol *51*, 371-384.

Martins, A., Ring, A., Omnus, D.J., Heessen, S., Pfirrmann, T., and Ljungdahl, P.O. (2019). Spatial and temporal regulation of the endoproteolytic activity of the SPS-sensor-controlled Ssy5 signaling protease. Mol Biol Cell *30*, 2709-2720.

Miller, E., Antonny, B., Hamamoto, S., and Schekman, R. (2002). Cargo selection into COPII vesicles is driven by the Sec24p subunit. EMBO J *21*, 6105-6113.

Miller, E.A., Beilharz, T.H., Malkus, P.N., Lee, M.C., Hamamoto, S., Orci, L., and Schekman, R. (2003). Multiple cargo binding sites on the COPII subunit Sec24p ensure capture of diverse membrane proteins into transport vesicles. Cell *114*, 497-509.

Nagamori, S., Smirnova, I.N., and Kaback, H.R. (2004). Role of YidC in folding of polytopic membrane proteins. J Cell Biol *165*, 53-62.

O'Keefe, S., and High, S. (2020). Membrane translocation at the ER: with a little help from my friends. FEBS J.

Ono, B.I., Ishino, Y., and Shinoda, S. (1983). Nonsense mutations in the can1 locus of Saccharomyces cerevisiae. J Bacteriol *154*, 1476-1479.

Rapoport, T.A., Li, L., and Park, E. (2017). Structural and Mechanistic Insights into Protein Translocation. Annu Rev Cell Dev Biol *33*, 369-390.

Risinger, A.L., Cain, N.E., Chen, E.J., and Kaiser, C.A. (2006). Activity-dependent reversible inactivation of the general amino acid permease. Mol Biol Cell *17*, 4411-4419.

Rosell, A., Meury, M., Alvarez-Marimon, E., Costa, M., Perez-Cano, L., Zorzano, A., Fernandez-Recio, J., Palacin, M., and Fotiadis, D. (2014). Structural bases for the interaction and stabilization of the human amino acid transporter LAT2 with its ancillary protein 4F2hc. Proc Natl Acad Sci U S A *111*, 2966-2971.

Rytka, J. (1975). Positive selection of general amino acid permease mutants in Saccharomyces cerevisiae. J Bacteriol *121*, 562-570.

Saier, M.H., Jr. (2000). Families of transmembrane transporters selective for amino acids and their derivatives. Microbiology *146 (Pt 8)*, 1775-1795.

Schoebel, S., Mi, W., Stein, A., Ovchinnikov, S., Pavlovicz, R., DiMaio, F., Baker, D., Chambers, M.G., Su, H., Li, D.*, et al.* (2017). Cryo-EM structure of the protein-conducting ERAD channel Hrd1 in complex with Hrd3. Nature *548*, 352-355.

Seinen, A.B., and Driessen, A.J.M. (2019). Single-Molecule Studies on the Protein Translocon. Annu Rev Biophys *48*, 185-207.

Serdiuk, T., Balasubramaniam, D., Sugihara, J., Mari, S.A., Kaback, H.R., and Muller, D.J. (2016). YidC assists the stepwise and stochastic folding of membrane proteins. Nat Chem Biol *12*, 911-917.

bioRxiv preprint doi: https://doi.org/10.1101/2020.07.05.188557; this version posted July 5, 2020. The copyright holder for this preprint (which was not certified by peer review) is the author/funder, who has granted bioRxiv a license to display the preprint in perpetuity. It is made available under aCC-BY-NC-ND 4.0 International license.

Serdiuk, T., Steudle, A., Mari, S.A., Manioglu, S., Kaback, H.R., Kuhn, A., and Muller, D.J. (2019). Insertion and folding pathways of single membrane proteins guided by translocases and insertases. Sci Adv *5*, eaau6824.

Sherwood, P.W., and Carlson, M. (1999). Efficient export of the glucose transporter Hxt1p from the endoplasmic reticulum requires Gsf2p. Proc Natl Acad Sci USA *96*, 7415-7420.

Shurtleff, M.J., Itzhak, D.N., Hussmann, J.A., Schirle Oakdale, N.T., Costa, E.A., Jonikas, M., Weibezahn, J., Popova, K.D., Jan, C.H., Sinitcyn, P.*, et al.* (2018). The ER membrane protein complex interacts cotranslationally to enable biogenesis of multipass membrane proteins. Elife *7*.

Silve, S., Volland, C., Garnier, C., Jund, R., Chevallier, M.R., and Haguenauer-Tsapis, R. (1991). Membrane insertion of uracil permease, a polytopic yeast plasma membrane protein. Mol Cell Biol *11*, 1114-1124.

Usami, Y., Uemura, S., Mochizuki, T., Morita, A., Shishido, F., Inokuchi, J., and Abe, F. (2014). Functional mapping and implications of substrate specificity of the yeast high-affinity leucine permease Bap2. Biochim Biophys Acta *1838*, 1719-1729.

van't Klooster, J.S., Bianchi, F., Doorn, R.B., Lorenzon, M., Lusseveld, J.H., Punter, C.M., and Poolman, B. (2020). Extracellular loops matter - subcellular location and function of the lysine transporter Lyp1 from Saccharomyces cerevisiae. FEBS J.

Volkmar, N., and Christianson, J.C. (2020). Squaring the EMC - how promoting membrane protein biogenesis impacts cellular functions and organismal homeostasis. J Cell Sci *133*.

Wagner, S., Pop, O.I., Haan, G.J., Baars, L., Koningstein, G., Klepsch, M.M., Genevaux, P., Luirink, J., and de Gier, J.W. (2008). Biogenesis of MalF and the MalFGK(2) maltose transport complex in Escherichia coli requires YidC. J Biol Chem *283*, 17881-17890.

Waterhouse, A.M., Procter, J.B., Martin, D.M., Clamp, M., and Barton, G.J. (2009). Jalview Version 2--a multiple sequence alignment editor and analysis workbench. Bioinformatics *25*, 1189-1191.

Wong, F.H., Chen, J.S., Reddy, V., Day, J.L., Shlykov, M.A., Wakabayashi, S.T., and Saier, M.H., Jr. (2012). The amino acid-polyamine-organocation superfamily. J Mol Microbiol Biotechnol *22*, 105-113.

Zhu, L., Kaback, H.R., and Dalbey, R.E. (2013). YidC protein, a molecular chaperone for LacY protein folding via the SecYEG protein machinery. J Biol Chem *288*, 28180-28194.

bioRxiv preprint doi: https://doi.org/10.1101/2020.07.05.188557; this version posted July 5, 2020. The copyright holder for this preprint (which was not certified by peer review) is the author/funder, who has granted bioRxiv a license to display the preprint in perpetuity. It is made available under aCC-BY-NC-ND 4.0 International license.

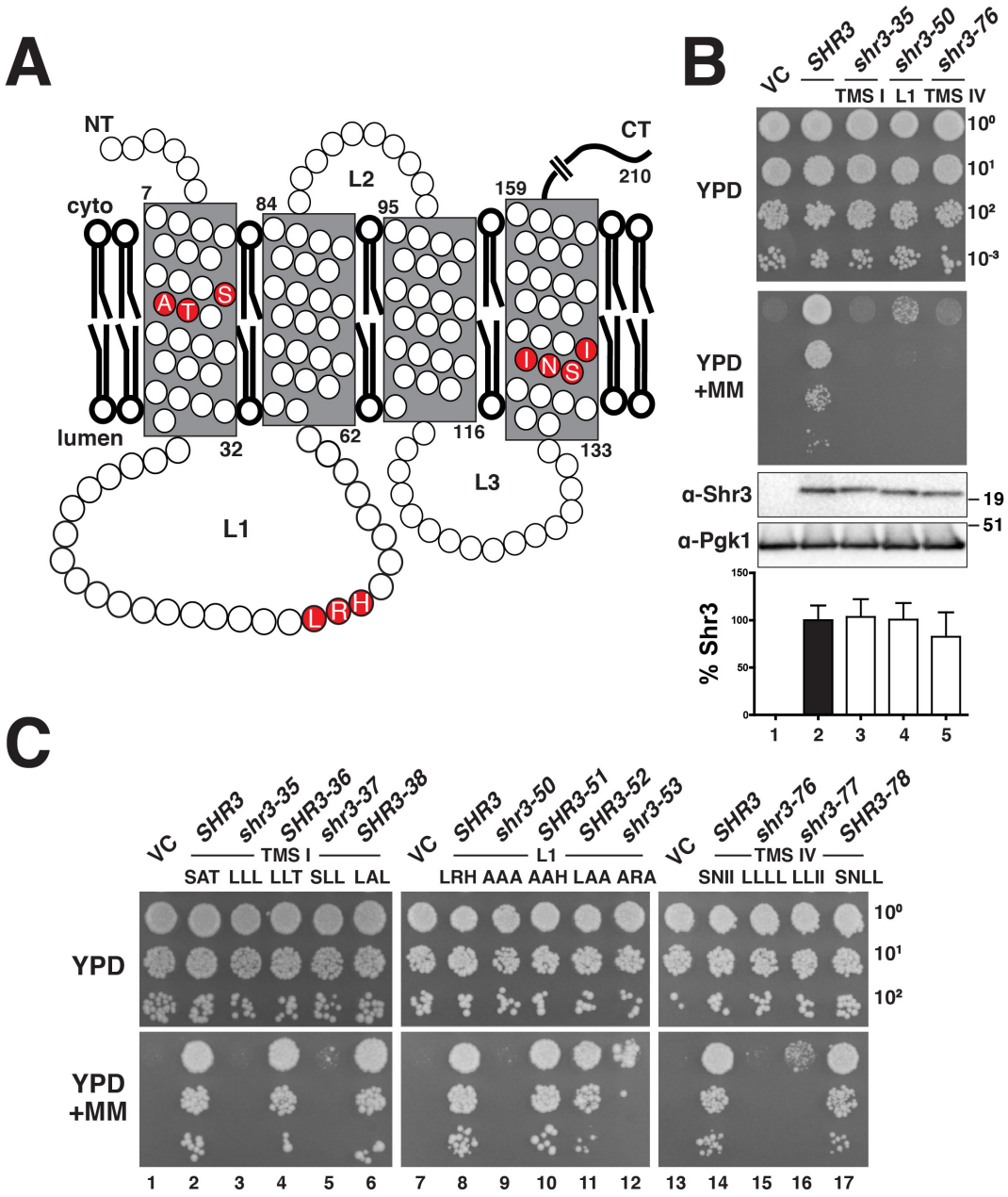

Figure 1. Scanning mutagenesis of the Shr3 membrane domain

(A) Graphical representation of Shr3 topology and position of residues resulting in a non-functional protein. (B) Top: Serial dilutions of cell suspensions from strain JKY2 (*shr3Δ*) carrying pRS316 (VC), pPL210 (*SHR3*), pAR4 (*shr3-35*), pAR18 (*shr3-50*) or pPL1349 (*shr3-76*) spotted on YPD and YPD+MM. The plates were incubated at 30 °C for 2 d and photographed. Bottom: Immunoblot analysis of Shr3 proteins in extracts prepared from the strains; the levels of Pgk1 were used as loading controls. The blots were developed using α-Shr3 and α-Pgk1 antibodies. The signal intensities of the immunoreactive forms of Shr3 and Pgk1 were quantified, and the Shr3 signals were normalized with respect to Pgk1; the mean values are plotted, error bars show standard deviation (n=3). (C) Serial dilutions of cell suspensions from strain JKY2 (*shr3Δ*) carrying pRS316 (VC), pPL210 (*SHR3*), pAR4 (*shr3-35*), pPL1330 (*SHR3-36*), pAR47 (*shr3-37*), pAR37 (*SHR3-38*), pAR18 (*shr3-50*), pAR51 (*SHR3-51*), pAR52 (*SHR3-52*), pAR50 (*shr3-53*), pPL1349 (*shr3-76*), pAR48 (*shr3-77*) or pAR49 (*SHR3-78*) spotted on YPD and YPD+MM plates. Plates were incubated at 30 °C for 2 d and photographed.

bioRxiv preprint doi: https://doi.org/10.1101/2020.07.05.188557; this version posted July 5, 2020. The copyright holder for this preprint (which was not certified by peer review) is the author/funder, who has granted bioRxiv a license to display the preprint in perpetuity. It is made available under aCC-BY-NC-ND 4.0 International license.

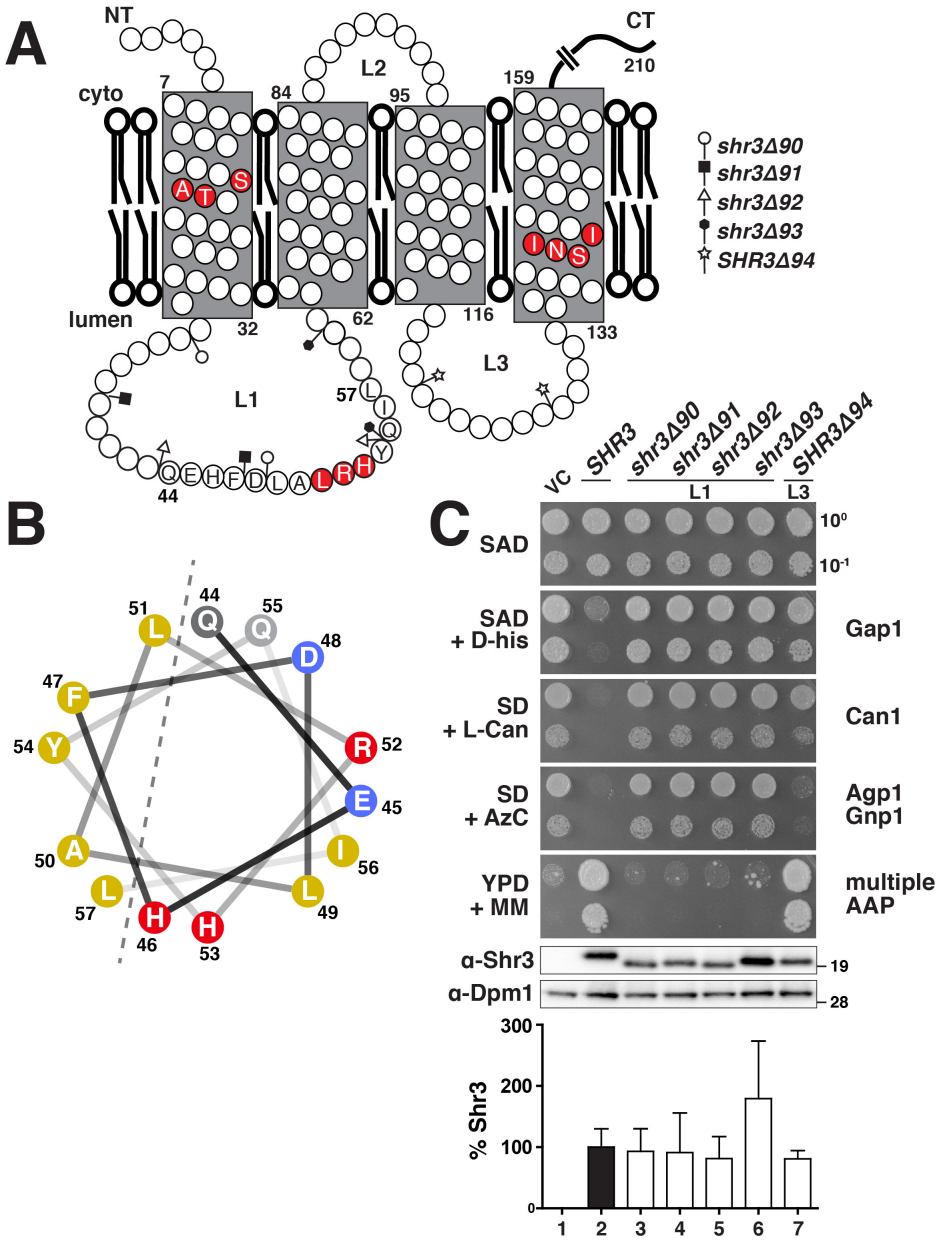

Figure 2. Deletion analysis of ER-lumen oriented loops

(A) Graphical representation of Shr3 topology and the positions of the internal deletions in loops L1 and L3. (B) Based on structural predictions (Drozdetskiy et al., 2015), amino acid residues 44-57 in L1 are predicted to fold into an α-helix with amphipathic character. Helical wheel projection of the L1 α-helix with non-polar (yellow), polar (grey), negatively- (blue) and positively-charged (red) residues indicated. (C) Serial dilutions of cell suspensions from strain JKY2 (*shr3Δ*) carrying pRS316 (VC), pPL210 (*SHR3*), pAR41 (*shr3Δ90*), pAR42 (*shr3Δ91*), pAR43 (*shr3Δ92*), pAR44 (*shr3Δ93*) or pAR45 (*shr3Δ94*) spotted on SAD containing D-histidine (D-his), SD + L-canavanine (L-Can), SD + AzC, and YPD + MM plates. Plates were incubated at 30 °C for 2 d and photographed. Bottom: Immunoblot analysis of Shr3 proteins in extracts prepared from the strains; the levels of Dpm1 were used as loading controls. The blots were developed using α-Shr3 and α-Dpm1 antibodies. The signal intensities of the immunoreactive forms of Shr3 and Dpm1 were quantified, and the Shr3 signals were normalized with respect to Dpm1; the mean values are plotted, error bars show standard deviation (n=3).

bioRxiv preprint doi: https://doi.org/10.1101/2020.07.05.188557; this version posted July 5, 2020. The copyright holder for this preprint (which was not certified by peer review) is the author/funder, who has granted bioRxiv a license to display the preprint in perpetuity. It is made available under aCC-BY-NC-ND 4.0 International license.

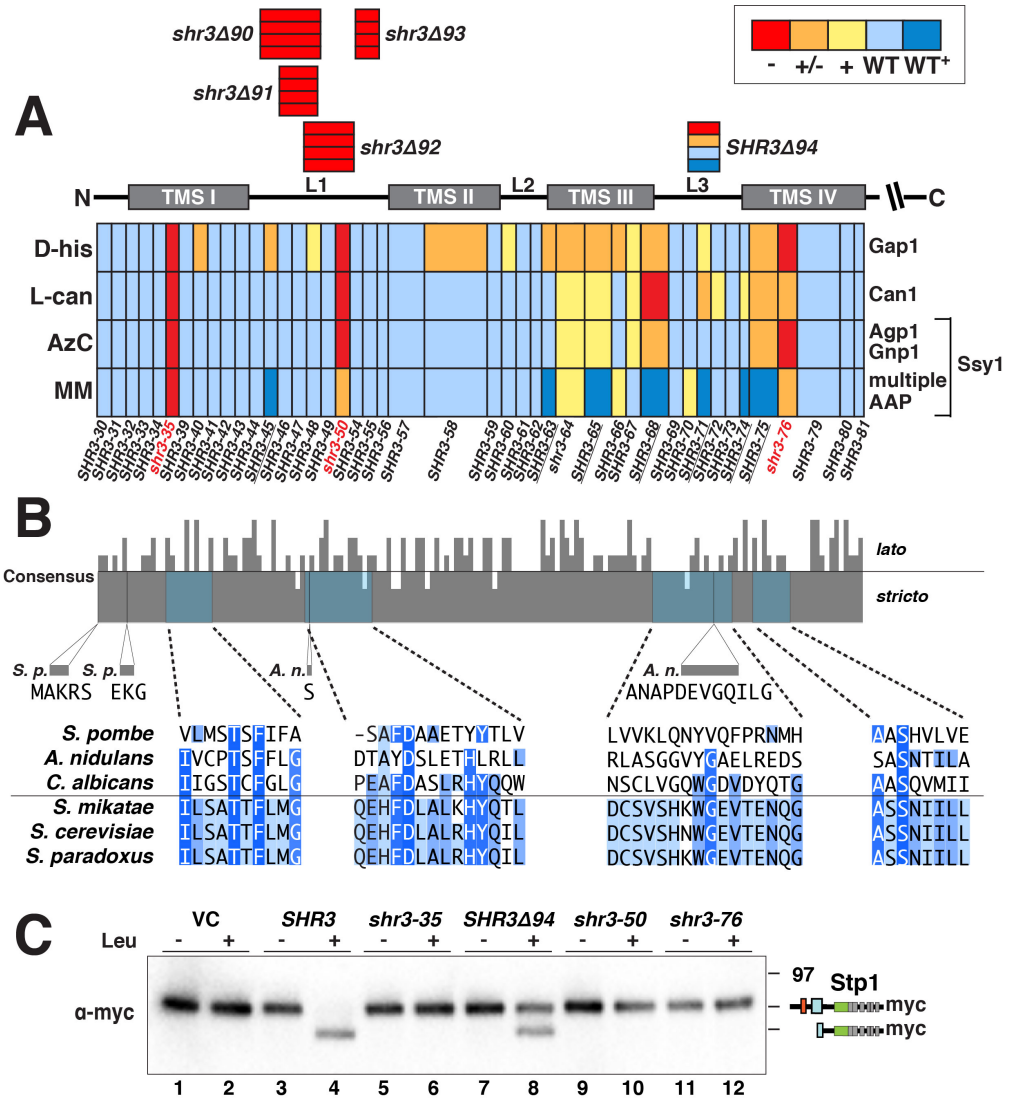

Figure 3. Mutational analysis of Shr3 function and substrate specificity

(A) Summary of growth characteristics of JKY2 (*shr3*Δ) individually expressing 44 Shr3-mutant proteins. Cells were spotted on media containing toxic amino analogues and nitrogen sources as follows: D-his, D-histidine (0.5% w/v), allantoin; L-can, L-canavanine (1 µg/ml), ammonium; AzC, azetidine-2-carboxylate (1 mM), ammonium; MM (200 µg/ml), yeast extract and peptone. Growth was scored after 2 - 3 d of incubation at 30 °C (Supplementary Materials Fig. S1-S10). Colors reflect Shr3 function relative to wildtype activity: red, no function (-); orange, weak but detectable function (+/-); yellow, intermediate function but less than wildtype (+); light blue, wildtype function (WT); dark blue, enhanced function (WT^{+}). (B) Clustal O (Madeira et al., 2019) comparison of Shr3 sequences, corresponding to aa residues 1-159 of *S. cerevisiae*, and orthologs of members from the *Saccharomyces sensu stricto* group (*S. paradoxus*, *S. mikatae*) and orthologs from *sensu lato* fungi (*S. pombe, A. nidulans,* and *C. albicans*). The consensus plot (identity; (Waterhouse et al., 2009) and detailed multiple sequence alignments are presented for the regions with mutations giving rise to major growth defects on selective media; identical residues in three (light blue), four (blue), and five or six homologs (dark blue) are highlighted. (C) Shr3-dependent Ssy1 folding and function assessed by Stp1 processing. Immunoblot analysis of extracts from FGY135 (*shr3*Δ) carrying pCA204 (*STP1-13xMYC*) and pRS316 (VC), pPL210 (*SHR3*), pAR004 (*shr3-35*), pAR45 (*SHR3Δ94*), pAR018 (*shr3-50*) or pPL1351 (*shr3-76*). Cells were grown in SD and induced 30 min with 1.3 mM leucine (+) as indicated.

bioRxiv preprint doi: https://doi.org/10.1101/2020.07.05.188557; this version posted July 5, 2020. The copyright holder for this preprint (which was not certified by peer review) is the author/funder, who has granted bioRxiv a license to display the preprint in perpetuity. It is made available under aCC-BY-NC-ND 4.0 International license.

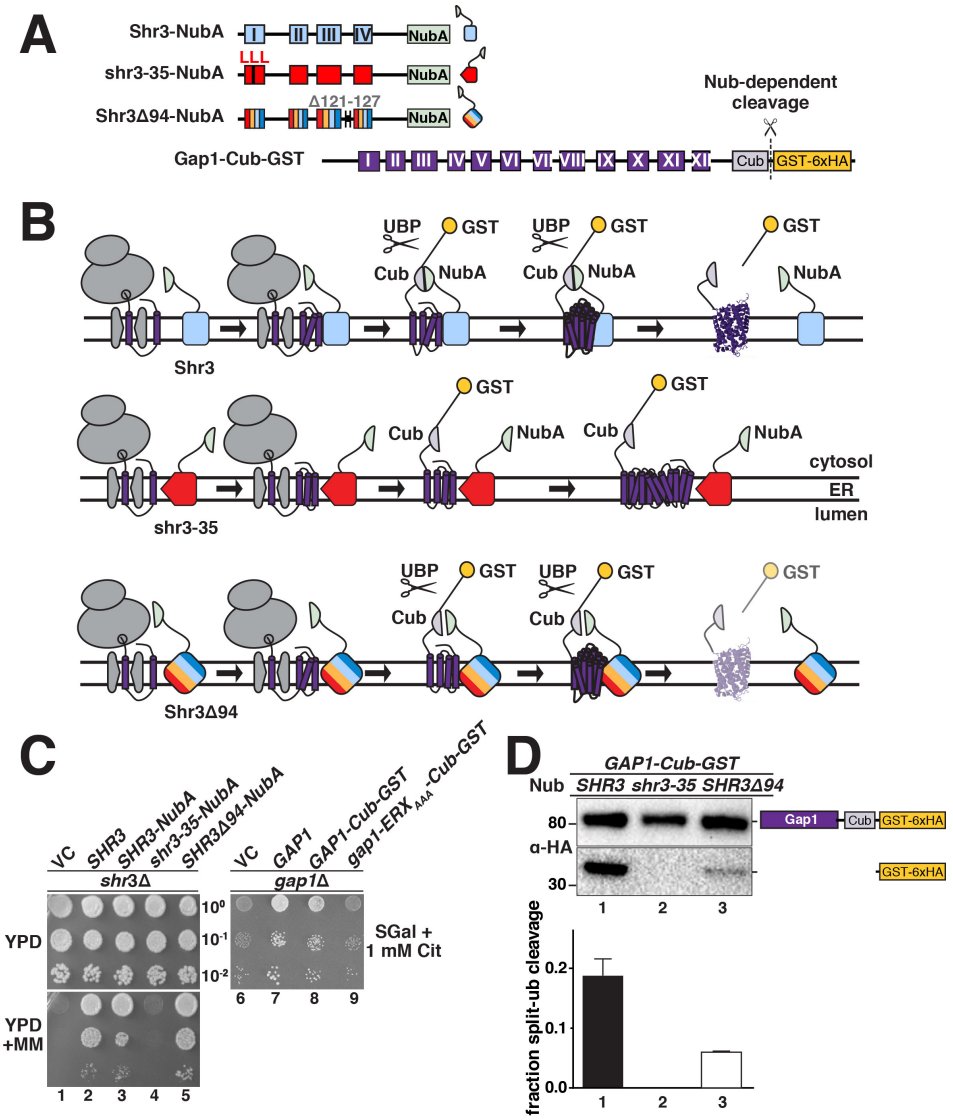

Figure 4. Assessing Shr3-Gap1 interactions using split ubiquitin

(A) Schematic diagram of the split ubiquitin Shr3-NubA, shr3-35-NubA, Shr3Δ94-NubA and Gap1-Cub-GST constructs. (B) Overview of the split-ubiquitin assay and expected outcomes. (C) Left panels: serial dilutions of cell suspensions from strain JKY2 (*shr3Δ*) carrying pRS316 (VC), pPL210 (*SHR3*), pPL1262 (*SHR3-NubA*), pAR67 (*shr3-35-NubA*) or pAR76 (*SHR3Δ94-NubA*) spotted on YPD and YPD+MM plates. Plates were incubated at 30 °C for 2 d and photographed. Right panel: serial dilutions of cell suspensions from strain FGY15 (*gap1Δ*) carrying pRS317 (VC), pJK92 (*GAP1*), pPL1257 (*GAP1-Cub-GST*) or pIM28 (*gap1-ERX$_{AAA}$-Cub-GST*) were spotted on minimal medium with 2 % galactose as carbon source and 1 mM L-citrulline as sole nitrogen source. Plates were incubated for 7 d and photographed. (D) Strain FGY135 (*gap1Δ shr3Δ*) expressing *SHR3-NubA* (pPL1262), *shr3-35-NubA* (pAR67) or *SHR3Δ94-NubA* (pAR76) and carrying pPL1257 (*GAP1-Cub-GST*) were induced with 2% galactose for 1 h. Proteins extracts were prepared, separated by SDS-PAGE and analyzed by immunoblotting using α-HA antibody. The signal intensities of the immunoreactive forms of full-length and cleaved Gap1 were quantified. The fraction of split-ubiquitin cleavage was determined; the mean values plotted with error bars showing standard deviation (n=3).

bioRxiv preprint doi: https://doi.org/10.1101/2020.07.05.188557; this version posted July 5, 2020. The copyright holder for this preprint (which was not certified by peer review) is the author/funder, who has granted bioRxiv a license to display the preprint in perpetuity. It is made available under aCC-BY-NC-ND 4.0 International license.

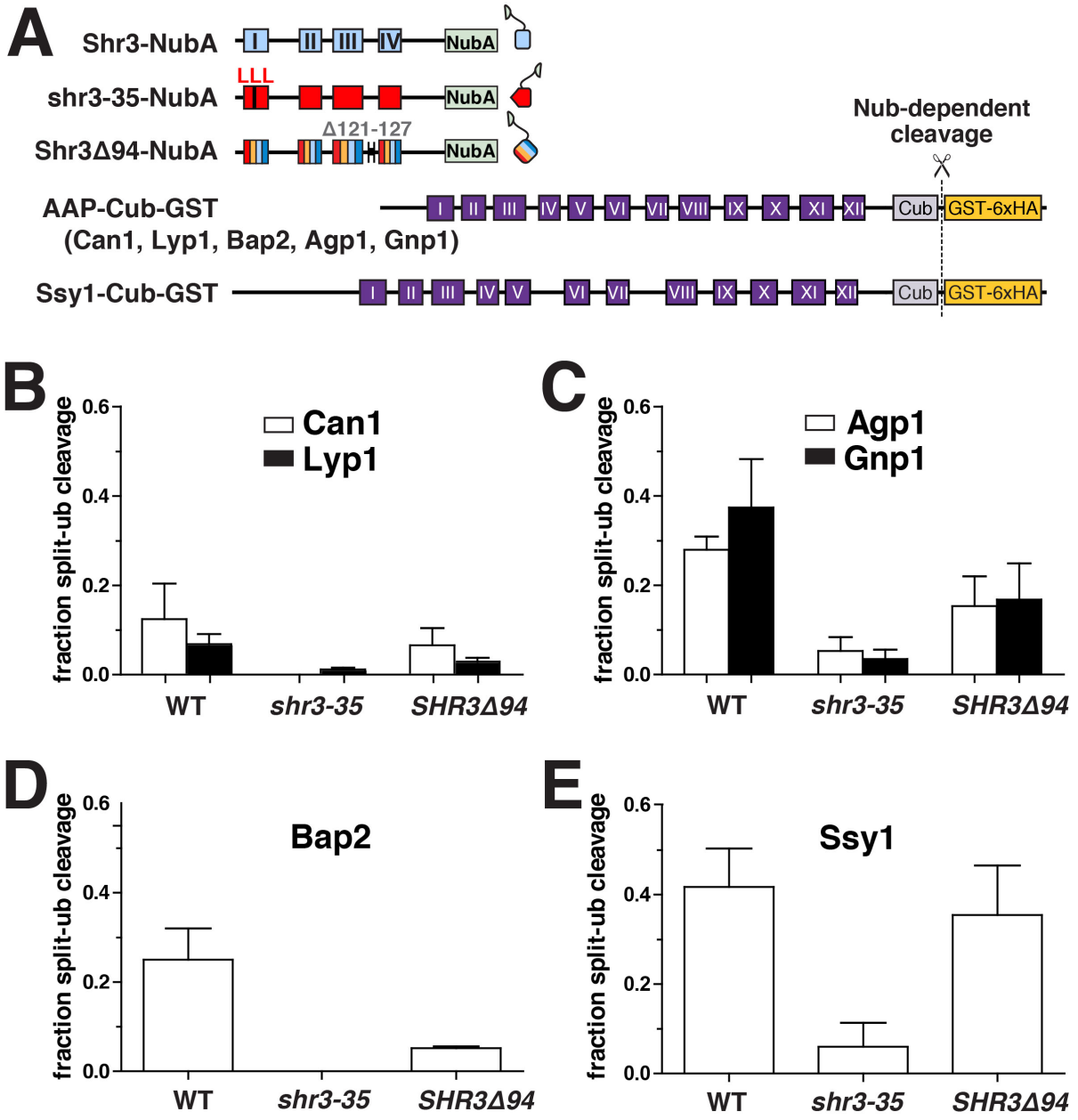

Figure 5. Shr3-AAP interactions

(A) Schematic diagram of the split ubiquitin constructs used to evaluate Shr3-AAP interactions. (B) Shr3-Can1 and Shr3-Lyp1 interactions. (C) Shr3-Agp1 and Shr3-Gnp1 interactions. (D) Shr3-Bap2 interactions. (E) Shr3-Ssy1 interactions. Strain FGY135 (*gap1Δ shr3Δ*) expressing *SHR3-NubA* (pPL1262), *shr3-35-NubA* (pAR67) or *SHR3Δ94-NubA* (pAR76) and carrying (B) pIM8 (*CAN1-Cub-GST*) or pIM18 (*LYP1-Cub-GST*), or (C) pIM6 (*AGP1-Cub-GST*) or pIM17 (*GNP1-Cub-GST*), or (D) pIM7 (*BAP2-Cub-GST*), or (E) pIM19 (*SSY1-Cub-GST*) were induced with 2% galactose for 1 h. Proteins extracts were prepared, separated by SDS-PAGE and analyzed by immunoblotting using α-HA antibody. The signal intensities of the immunoreactive forms of full-length and cleaved Can1, Lyp1, Agp1, Gnp1, Bap2 and Ssy1 constructs were quantified. The fraction of split-ubiquitin cleavage was determined; the mean values plotted with error bars showing standard deviation (n=3).

bioRxiv preprint doi: https://doi.org/10.1101/2020.07.05.188557; this version posted July 5, 2020. The copyright holder for this preprint (which was not certified by peer review) is the author/funder, who has granted bioRxiv a license to display the preprint in perpetuity. It is made available under aCC-BY-NC-ND 4.0 International license.

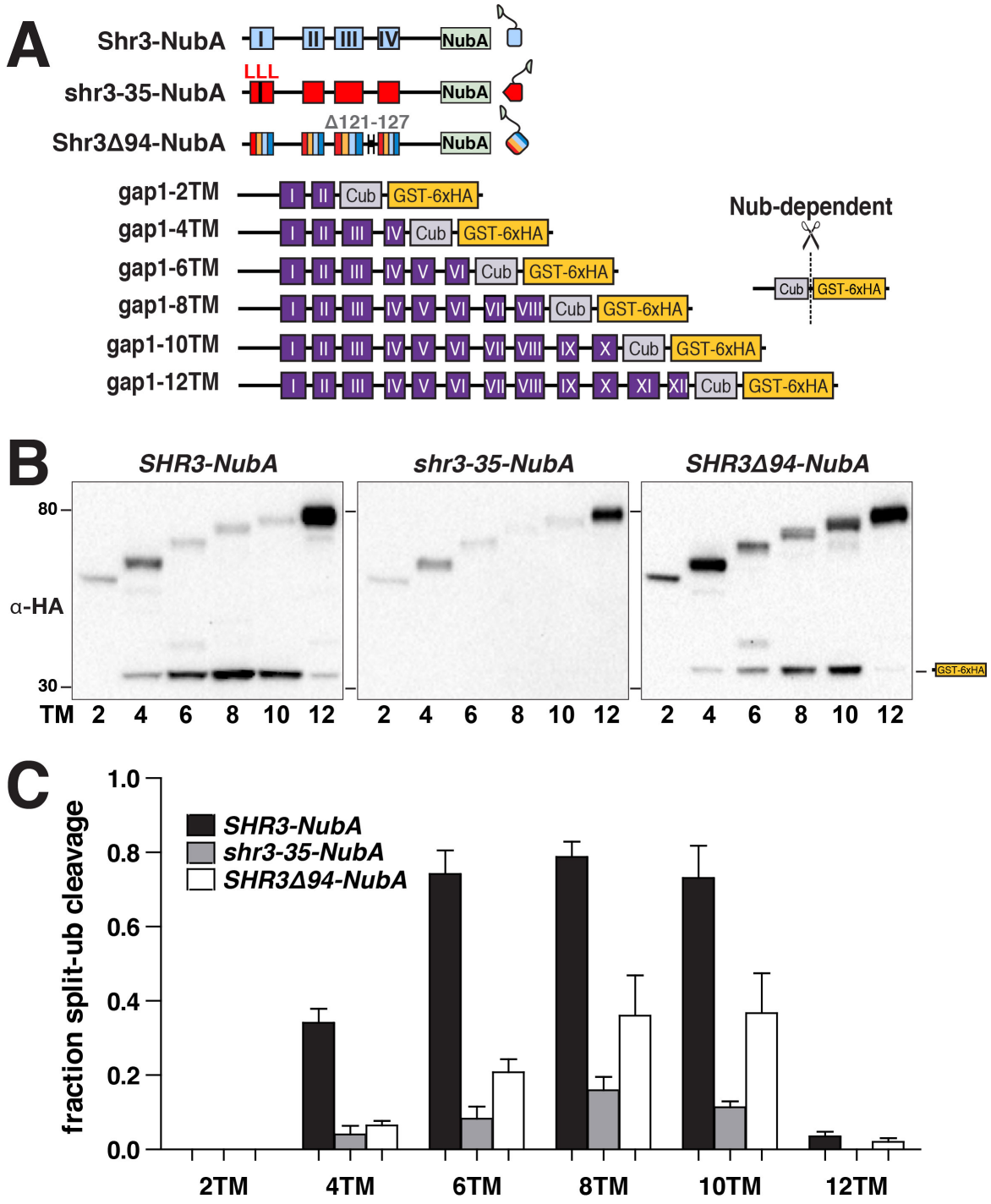

Figure 6. Temporal Shr3-Gap1 chaperone-substrate interactions

(A) Schematic diagram of split ubiquitin constructs including the gap1-Cub-GST truncation alleles. (B) Strain FGY135 (*gap1Δ shr3Δ*) carrying pIM1 (gap1-2TM-Cub-GST), pIM2 (gap1-4TM-Cub-GST), pIM3 (gap1-6TM-Cub-GST), pIM4 (gap1-8TM-Cub-GST), pIM5 (gap1-10TM-Cub-GST) or pIM16 (gap1-12TM-Cub-GST) and pPL1262 (*SHR3-NubA*)(left panel), pAR67 (*shr3-35-NubA*) (center panel) or pAR76 (*SHR3Δ94-NubA*)(right panel) were induced with 2% galactose for 1 h. Extracts were prepared, separated by SDS-PAGE and analyzed by immunoblotting using α-HA antibody. The signal intensities of the immunoreactive forms of uncleaved Cub constructs and cleaved interaction marker (GST-6xHA) were quantified; the mean values of the fraction of split ubiquitin cleavage is plotted with error bars showing standard deviation (n=3).

bioRxiv preprint doi: https://doi.org/10.1101/2020.07.05.188557; this version posted July 5, 2020. The copyright holder for this preprint (which was not certified by peer review) is the author/funder, who has granted bioRxiv a license to display the preprint in perpetuity. It is made available under aCC-BY-NC-ND 4.0 International license.

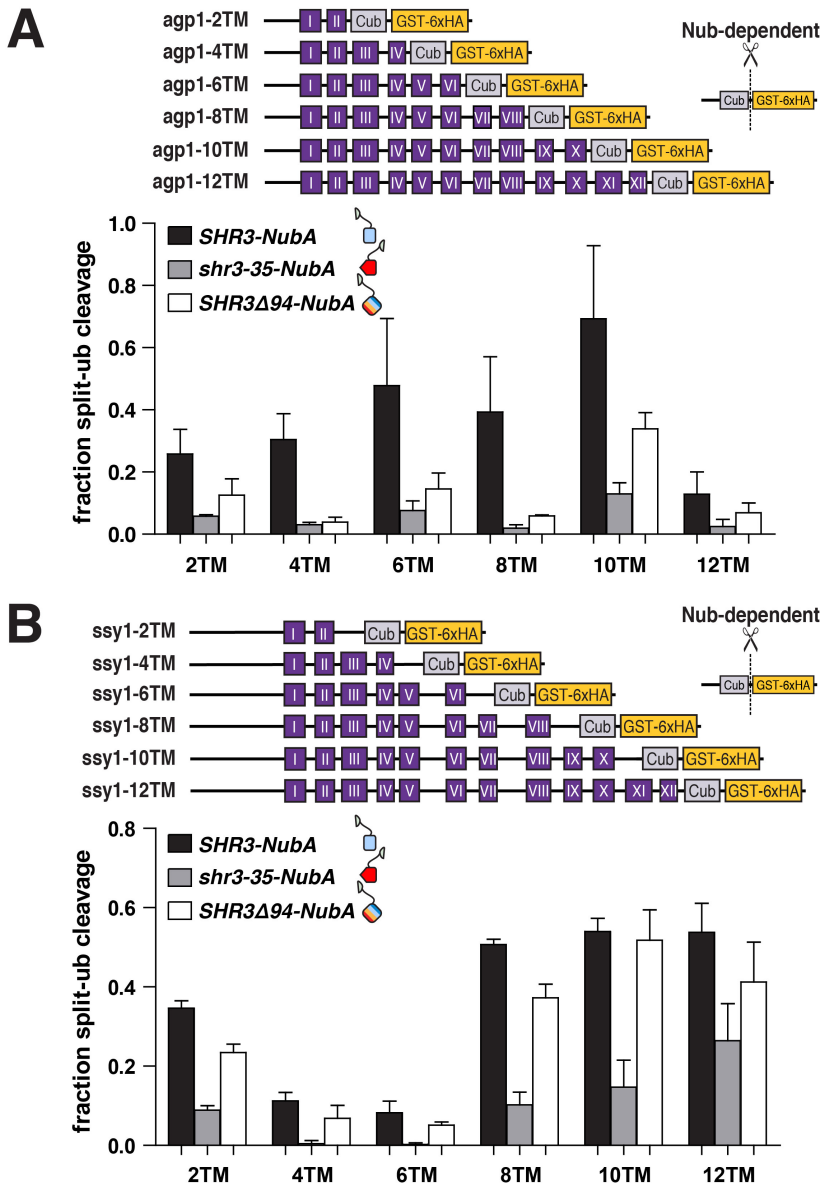

Figure 7. Temporal Shr3-Agp1 and Shr3-Ssy1 chaperone-substrate interactions

(A) Schematic diagram of agp1-Cub-GST truncation constructs. Strain FGY135 (*gap1Δ shr3Δ*) expressing *SHR3-NubA* (pPL1262), *shr3-35-NubA* (pAR67) or *SHR3Δ94-NubA* (pAR76) and carrying pIM9 (agp1-2TM-Cub-GST), pIM10 (agp1-4TM-Cub-GST), pIM11 (agp1-6TM-Cub-GST), pIM12 (agp1-8TM-Cub-GST), pIM13 (agp1-10TM-Cub-GST) or pIM26 (agp1-12TM-Cub-GST) were induced with 2% galactose for 1 h. Extracts were prepared, separated by SDS-PAGE and analyzed by immunoblotting using α-HA antibody. The signal intensities of the immunoreactive forms of uncleaved Cub constructs and cleaved interaction marker (GST-6xHA) were quantified; the mean values of the fraction of split ubiquitin cleavage is plotted with error bars showing standard deviation (n=3). (B) Schematic diagram of ssy1-Cub-GST truncation constructs. Strain FGY135 (*gap1Δ shr3Δ*) expressing *SHR3-NubA* (pPL1262), *shr3-35-NubA* (pAR67) or *SHR3Δ94-NubA* (pAR76) and carrying pIM20 (ssy1-2TM-Cub-GST), pIM21 (ssy1-4TM-Cub-GST), pIM22 (ssy1-6TM-Cub-GST), pIM23 (ssy1-8TM-Cub-GST), pIM24 (ssy1-10TM-Cub-GST) or pIM25 (ssy1-12TM-Cub-GST) were induced with 2% galactose for 1 h. Extracts were prepared, and analyzed as in (A) and the mean values of the fraction of split ubiquitin cleavage is plotted with error bars showing standard deviation (n=3).

bioRxiv preprint doi: https://doi.org/10.1101/2020.07.05.188557; this version posted July 5, 2020. The copyright holder for this preprint (which was not certified by peer review) is the author/funder, who has granted bioRxiv a license to display the preprint in perpetuity. It is made available under aCC-BY-NC-ND 4.0 International license.

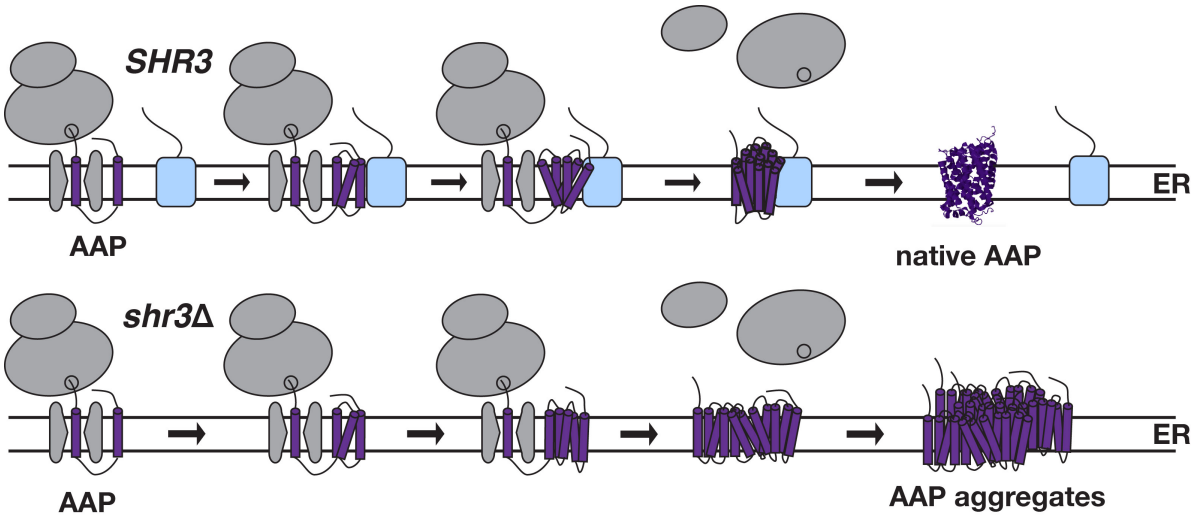

Figure 8. Model of Shr3 facilitated AAP folding

Shr3 interacts transiently with AAP as they are co-translationally inserted into the ER membrane. Interactions start early, when 2-4MS have partitioned into the lipid bilayer, and continue until all MS are inserted. When AAP have fully integrated into the membrane and attain native conformations, the interactions with Shr3 diminish. The co-translational Shr3 function is specifically required for AAP folding and ER-exit. The chaperone activity depends on relatively few residues of the Shr3 sequence, suggesting that it functions as folding template. In the absence of Shr3, AAP are specifically retained in the ER and form high-molecular weight aggregates that are recognized as ERAD substrates.

bioRxiv preprint doi: https://doi.org/10.1101/2020.07.05.188557; this version posted July 5, 2020. The copyright holder for this preprint (which was not certified by peer review) is the author/funder, who has granted bioRxiv a license to display the preprint in perpetuity. It is made available under aCC-BY-NC-ND 4.0 International license.

Supplementary Material

Figures:

Tables: